UiT The Arctic University of Norway

Faculty of Engineering Science and Technology, Department of Electrical Engineering

Real-time application of grid-forming converters in smart distribution network

Jon-Kristian Leirvang

Master's thesis in Electrical Engineering, ELE-3900, May 2023

Abstract

As the world faces the urgent need to reduce greenhouse gas emissions and combat climate change, renewable sources of energy have emerged as a viable solution. However, integrating renewable energy into existing power grids poses unique challenges. The availability of solar power depends on sunlight, wind power on wind speed, and this variability can cause instability and fluctuations in the grid, affecting its reliability and performance. Grid-forming converters can overcome this challenge by emulating the behavior of synchronous generators. They control the voltage, frequency, and phase angle of the electricity generated by renewable sources, allowing them to operate in a grid-independent manner. Due to its complex power system dynamics, it is useful to test the systems behavior, which can be achieved with a real-time simulator.

In this thesis a study upon four grid-forming converters mathematical model, power dynamics, frequency regulation through a control application and their ability to reach stability is addressed within a nine-bus system. Testing of the research models is done in MATLAB/Simulink and RT-LAB to achieve a broader understanding of the grid-forming converters contribution.

Keywords: RT-LAB, Simulink, Grid-forming converters, nine-bus, renewable energy, power system stability.

Acknowledgement

This thesis is a result of a two-year master program at UiT the Arctic University of Norway - Campus Narvik. I would like to thank all professors throughout the years for immense learning outcomes, a special thanks goes to Pawan Sharma and Raju Wagle for providing this thesis with the ideas. Additionally, I would like to thank my family and my better half for being patient with me through this last semester.

Table of Contents

List of Tables

List of Figures

1 Introduction

1.1 Background

UiT the Arctic University of Norway – Campus Narvik has a real-time simulator from Opal RT. This device enables testing of dynamic power system simulations from MATLAB/Simulink models to assess their performance in real-time scenarios before integrating them into a grid. This capability is particularly valuable for grid owners worldwide who are planning to incorporate a significant portion of renewable energy sources like wind and solar. Furthermore, this real-time simulator can greatly enhance our understanding of the behavior of grid-forming converters in real-time situations. Additionally, analyzing complex power systems through problem-solving in a real-time simulator provides valuable insights into the behavior of power dynamics which can give valuable learning outcomes for further work on this topic at this faculty.

1.2 Problem description

Due to the increasing number static power electronics converters of renewable energy sources in a distribution network, the grid will have low inertia grid. The limited amount of inertial of the grid make the system vulnerable to uncertain network dynamics. Grid-forming converters are one of the solutions in solving the problem by providing the virtual inertia to the grid. In this project work, a framework for real-time application of grid-forming converter is proposed. Application of grid-forming converter on IEEE 9 bus system will be modeled and tested on Opal RT in real-time.

Objectives

- Literature survey of different types of grid-forming converters in smart distribution network.
- Classification of different type of control schemes implemented in grid-forming converter and different setups for real-time simulations.
- Implement a control application in grid-forming converter.
- Propose a real-time implementation of grid-forming converter in nine bus system.

1.3 Previous work

A literature study based upon four different grid forming converters was done in the fall, it had the same general problem as the description of the master thesis except implementing a control application in the grid-forming converters and proposing a real-time implementation of converters in the nine-bus system. The models were provided by A. Tayebi and tested in Simulink [1]. The main goal was to dig deeper into how the grid forming converters will operate in smart distribution networks and how they can provide virtual inertia to the grid. Due to the short amount of time, there were only provided a small literature survey, this thesis will take a broader approach to this.

1.4 Scopes and limitations

The task of this thesis is to develop real-time simulations of grid-forming converters, which have been achieved using RT-LAB software. The focus is on integrating a nine-bus system with a control application that is compatible with this software. All the dynamics and models are built in a MATLAB/Simulink environment, and their restraining is closely connected to the entire project. The main tasks of the project have been attempted to be fulfilled within the limitations imposed by the RT-LAB software. These limitations are associated with experiences to these software and power dynamics behavior.

2 Theory

2.1 Power system Stability

In order to have grid forming converters to operate smoothly and integrate it to a grid it is necessary to investigate power system stability. Power system stability refers to the ability of a power system to maintain a steady state or return to a steady state after a disturbance or change in the operating conditions. The stability of a power system is critical to its reliable operation and is an important consideration for transmission system operators [2], [3, p. 9].

Essential power system stability features to obtain stability for grid-forming converters:

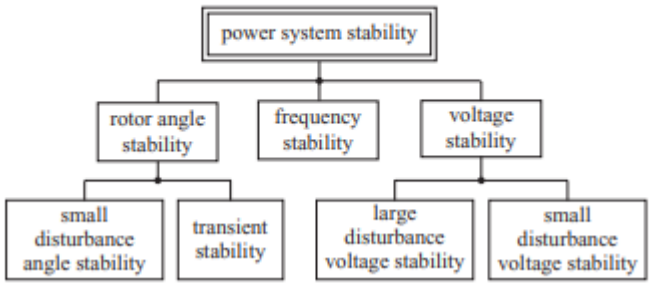

Figure 1 - Classification of power system stability

- Steady-state stability: This refers to the ability of a power system to maintain a steady-state operating condition when there are no disturbances.
- Rotor angle stability: This refers to the ability of a power system to maintain synchronism and stability under small disturbances, such as small changes in load or generation.
- Transient stability: This refers to the ability of a power system to maintain synchronism after a large disturbance, such as a fault or a sudden change in load.

- Frequency stability: This refers to the degree to which an oscillating signal produces the same frequency for a specified interval of time.

- Voltage stability: This refers to the ability of a power system to maintain a steady voltage profile under changing operating conditions.

Maintaining power system stability requires careful planning and operation of the system. This can include the use of automatic voltage regulators, load shedding schemes, and other control measures to ensure that the power system remains stable and reliable. Additionally, transmission system operators must continuously monitor the system and respond quickly to any disturbances through various regulations to prevent instability and potential blackouts [2], [4].

2.1.1 Rotor angle stability

Rotor angle stability is a type of dynamic stability that refers to the ability of a power system to maintain synchronism between its generators and the power grid. In other words, it refers to the ability of the generator sources in a power system to maintain a constant relative phase angle with respect to each other and the grid. This is important for the smooth and stable operation of the power system and to prevent disturbances from causing large power swings or blackouts.

When a disturbance occurs in the power system, such as a fault or a sudden change in load, the generators may experience a change in rotor angle due to the transient response of the system [5, pp. 18-27]. If this change in rotor angle and power is large enough, it can lead to a loss of synchronism between the generators and the power grid, which can cause the generators to fall out of synchronism and trip offline from the grid, resulting in a blackout. This is often referred to the transient stability [5, p. 827].

2.1.2 Frequency stability

In a power system, the frequency is determined by the balance between the power generation and the power consumption. If the power consumption increases, the system frequency will decrease, and if the power generation increases, the system frequency will increase. Therefore, maintaining frequency stability is important for the reliable and efficient operation of the power system.

If the frequency deviates too much from the nominal frequency, it can cause damage to equipment and may result in power outages. In extreme cases, large frequency deviations can lead to cascading failures that can cause blackouts over wide areas. To maintain frequency stability, transmission system operators use various control measures, such as load shedding and frequency regulations to achieve equilibrium between generation and consumption [3], [6, pp. 335-340].

2.1.2.1 Dynamic performance metrics

Two key metrics for measuring frequency dynamic performance are the rate of change of frequency and frequency nadir. Rate of change of frequency measures the speed of frequency change resulting from a sudden load-generation imbalance. It is calculated by dividing the difference between two frequency measurements taken over a window of time typically 0.1-0.5 seconds. Rate of change of frequency is expressed in Hz/second and is used as a trigger index for generator protection. The chosen window of time is such that the response to the disturbance is mainly influenced by the system inertia response before the majority of turbine governors react. Meanwhile, frequency nadir represents the lowest frequency reached after the disturbance and is important for evaluating frequency dynamic performance, particularly in relation to underfrequency load shedding schemes [7].

In traditional power systems, rate of change of frequency is a critical factor because it is directly related to the system's inertia level, which is closely tied to transient stability. The slow response rate of most turbine-governor systems for synchronous generators is responsible for the strong correlation between the inertia level and transient stability. However, in an inverter-based resource dominated system, where inverter-based resources have fast response capabilities and different dynamics, research upon it suggest the rate of change of frequency may not always serve as an accurate indicator of system stability [7], [8].

The equation for rate of change of frequency can be expressed as follows.

$$RoCoF_{\tau} = \frac{\|f_{\tau} - f_0\|}{\tau} \quad (1)$$

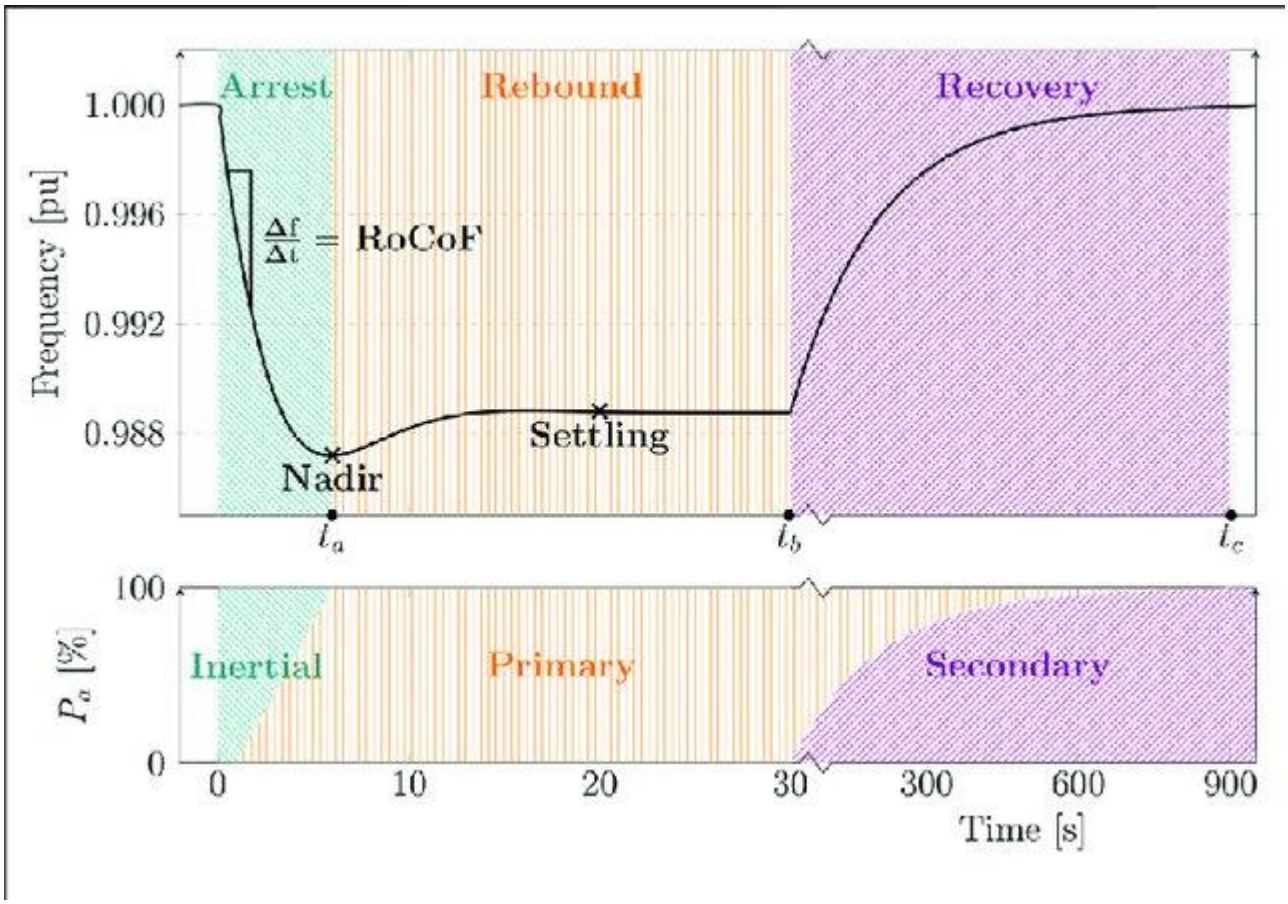

Figure 2 - Frequency regulation [9].

2.1.2.2 Frequency regulations

The use of these frequency regulations is becoming increasingly important as more variable renewable energy sources, such as wind and solar, are integrated into the power system. These sources can cause rapid changes in the power output, which can lead to frequency deviations. European transmission system operators, operates with a process when an imbalance occurs in the grid with the following steps. The first process, Fast frequency response, occurring seconds after the disturbance, then Frequency containment reserves is activated to bring the frequency back to a new steady state. In order to bring the frequency back to the nominal state, the Frequency restoration reserves are activated when the last disturbance is handled. When designing frequency regulations, it is necessary to not use the same generating source for two or more regulation to ensure enough reserves is available if another disturbance occurs [10], [11].

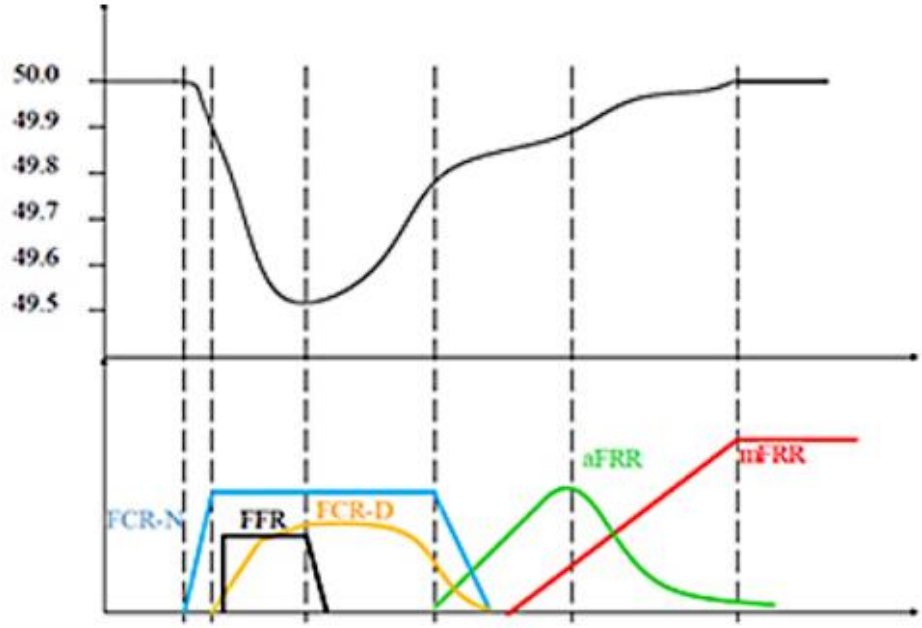

Figure 3 - frequency regulation over time [12, fig. 5].

2.1.2.3 Frequency containment reserves

Frequency containment reserves is the primary reserve, this reserve is used to address sudden changes in the power demand automatically. This is provided with generators already online and running in the grid at less of their full capacity. The frequency containment reserve in Nordic system is operating with two different states, Frequency containment reserves for normal operations and Frequency containment reserves for disturbances, to move the frequency towards equilibrium during normal operation and disturbances. Consider the nominal frequency for Nordic systems, then the frequency containment reserves for normal operations, operates in the range of 49,5 Hz to 50,1 Hz and must be capable for up and down regulation. Frequency containment reserves for disturbances, operates in the range of 49,5 to 50,5 for limiting the frequency deviation, this is divided into separate up- and downregulation products [13].

2.1.2.4 Fast frequency reserve

Fast frequency reserve is a secondary reserve and is designed to respond to frequency deviations that occur within a few cycles of the nominal frequency, typically on the order of a few milli seconds after a disturbance depending on the deviation. It acts like a compliment to the Frequency containment reserves and need to support for at least 5 seconds [10, p. 7].

Fast frequency reserve is provided by generators or energy storage systems that can rapidly increase or decrease to handle low-inertia situations. In other words, this means the stored kinetic energy in the rotating masses in the generating system resists changes in frequency.

This must be accordingly to the dimension principle to which the loss of a generation unit or high voltage direct current link must not cause the frequency to drop below 49,0 Hz. Then the volume needed for the Fast frequency reserve depends on the possible inertia from the size of the reference incident. After handling the fault, the reserve unit must be able to reactivate in short amount of the time to handle future disruptions [14].

2.1.2.5 Frequency restoration reserve

The main difference between automatic- and manual frequency restoration reserve besides being categorized secondary and tertiary reserves, is the speed of their response time and volume. automatic frequency restoration is constructed to respond very quickly and automatically to frequency deviations, which makes it more effective at maintaining the stability of the grid during sudden changes in demand or supply. and manual frequency restoration reserve, on the other hand, is more constructed for responding to slower changes in demand or supply that may require a more measured and deliberate response. Both get an activation signal from the transmission system operator when and how much to contribute to the grid [12], [15], [16].

2.1.3 Voltage stability

Voltage stability refers to the ability of a power system to maintain a stable voltage profile under normal operating conditions and after a disturbance. In other words, it refers to the ability of the power system to maintain a constant voltage at all buses in the system, despite changes in the system load and generation.

In a power system, the voltage level at each bus is affected by various factors, such as the power generation, the load demand, and the electrical impedance of the transmission lines and transformers.

To maintain voltage stability, Transmission system operators use various control measures, such as reactive power control through reactive compensation, voltage regulation, and load shedding, to regulate the voltage level at each bus and ensure that it remains within acceptable limits. Mostly this is achieved through the excitation of the synchronous machine, further steps will be discussed about how the converter-based generation sources can achieve this [3], [17].

2.2 Generator control

2.2.1 Governor

A turbine governor is a device that regulates the flow of fluid into a turbine in a power plant to maintain a constant generator speed and output power. It is typically a mechanical or electronic system that senses the rotational speed of the turbine shaft and adjusts the position of the turbine control valves to control the flow of fluid into the turbine.

The governor is an important component of the power plant control system, as it helps to maintain system stability by responding to changes in power demand from the electrical load. If the power demand from the load increases, the governor will increase the flow of fluid into the turbine to maintain the generator speed and output power. Similarly, if the load decreases, the governor will reduce the flow of fluid into the turbine to prevent the generator from overspeeding.

There are various types of turbine governors, including mechanical-hydraulic governors, electronic governors, and electro-hydraulic governors. Mechanical-hydraulic governors are the oldest type of governor and use mechanical linkages and hydraulic actuators to control the turbine valves. Electronic governors use electronic sensors and control systems to adjust the turbine valves, while electro-hydraulic governors combine electronic sensors with hydraulic actuators [3, pp. 25-34], [5, pp. 399-448].

In addition, a wind turbine “governor” is a control system that regulates the rotational speed of a wind turbine rotor to optimize energy capture and maintain system stability. In other words, the governor responds to changes in wind speed and power demand by adjusting the pitch angle of the blades to maintain a constant generator speed and output power. This helps to prevent the generator from overspeeding or underspeeding, which can lead to system instability and potential damage to the generator unit and its power electronics [3, pp. 482-484].

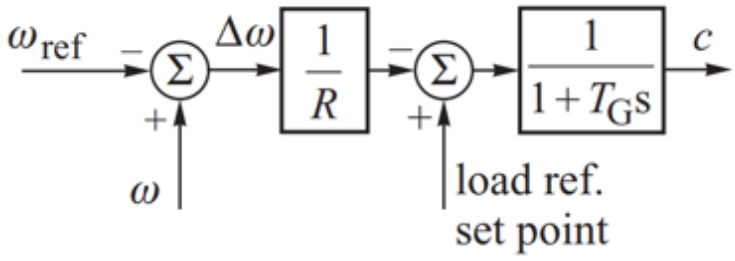

Figure 4 - Static and dynamic properties of the turbine–governor system [3, fig. 2.14].

The mechanical power output in Figure 4 is provided with the change in speed through the coefficient R, which corresponds to the gain the droop percentage and the transfer function is the effective governor time constant [3, p. 32].

2.2.2 Excitation system

The excitation system of a generator is made up of two key components: the exciter and the automatic voltage regulator. This system is essential for providing the necessary DC field current to the generator. The exciters can be categorized into rotating or static exciters. The rotating exciters consist of the output of a DC generator or rectified AC power source which is used to supply the required DC current to the field winding. Modern high-power generators often use static exciters, which are rectifiers that use thyristors or other solid-state components such as diodes to provide the required DC current to the field winding. The Automatic Voltage Regulator is responsible for controlling the amount of current supplied by the exciter to the generator's field winding, which in turn regulates the terminal voltage of the generator [3].

2.2.3 Power system stabilizer

The main idea behind Power System Stabilizer is to improve the stability of a power system by modifying the excitation of the generator. As mentioned the excitation system is responsible for controlling the voltage of the generator, and the Power System Stabilizer is used to modulate the excitation system in response to changes in the system frequency or other disturbances.

In a typical power system, the generators that are connected to the grid is required to maintain a constant frequency and voltage. When there is a disturbance in the system, such as a sudden change in load or a fault, the system can become unstable, leading to frequency and voltage fluctuations. A Power System Stabilizer can help to dampen these oscillations by adjusting

the excitation system of the generator by adding a measured feedback signal that is in phase with the change in rotor speed [3].

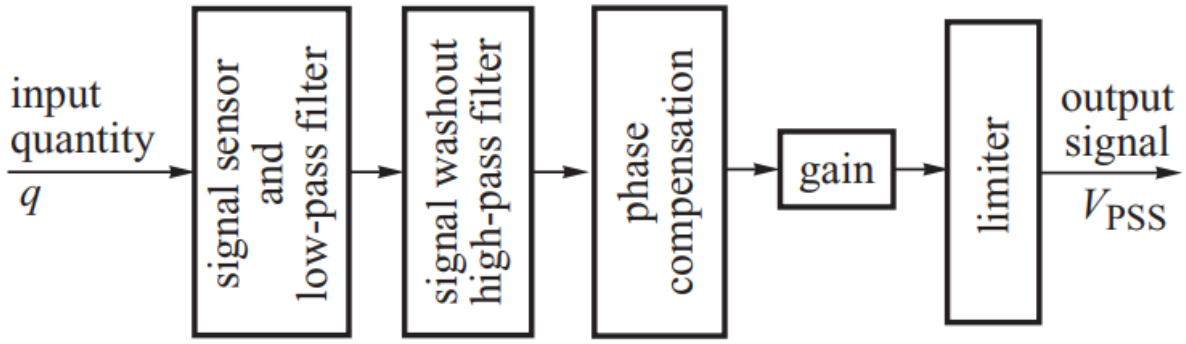

Figure 5 – power system stabilizer [3].

The design of phase compensation needs carefully tuning, so it is important to consider the phase shift caused by both the input signal and the low- and high pass filters. In certain scenarios the filters can be designed in a such way that the output signal produces a total phase shift of net zero for the frequency of rotor oscillations [3].

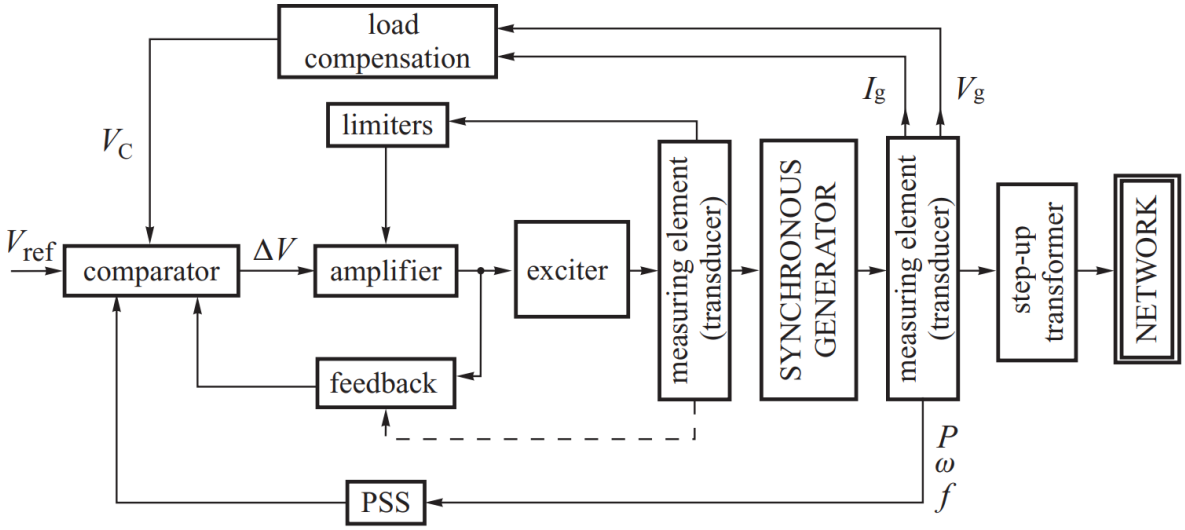

Figure 6 - Block diagram of the excitation, AVR system and power system stabilizer [3].

2.2.4 Reference frames

2.2.4.1 Park an inverse park

In power systems, time-varying phasor models are generally considered accurate as long as the phasors change slowly relative to the system frequency. However, when examining rapid dynamic events, quasi-static phasor assumptions may not be precise, and may require studies on transient models based on abc or $dq0$ quantities. The $dq0$ transformation and time-varying phasors maps sinusoidal signals to constants. Moreover, the $dq0$ transformation offers an accurate representation of both transient and static signals at steady state and does not rely on the assumption of a quasi-static network. The results produce well-defined equilibrium points, and $dq0$ models are beneficial for analyzing complex transients in fast dynamic phenomena [18].

The general form of converting the time-domain components of a three-phase system in an abc reference frame to direct, quadrature, and zero components in a rotating reference frame aligned to the q-axis.

$$T_p = \begin{bmatrix} d \\ q \\ 0 \end{bmatrix} = \frac{2}{3} \begin{bmatrix} \sin(\theta) & \sin\left(\theta - \frac{2\pi}{3}\right) & \sin\left(\theta + \frac{2\pi}{3}\right) \\ \cos(\theta) & \cos\left(\theta - \frac{2\pi}{3}\right) & \cos\left(\theta + \frac{2\pi}{3}\right) \\ \frac{1}{2} & \frac{1}{2} & \frac{1}{2} \end{bmatrix} \begin{bmatrix} a \\ b \\ c \end{bmatrix} \tag{2}$$

$$T_p^{-1} = \begin{bmatrix} a \\ b \\ c \end{bmatrix} = \begin{bmatrix} \sin(\theta) & \cos(\theta) & 1 \\ \sin\left(\theta - \frac{2\pi}{3}\right) & \cos\left(\theta - \frac{2\pi}{3}\right) & 1 \\ \sin\left(\theta + \frac{2\pi}{3}\right) & \cos\left(\theta + \frac{2\pi}{3}\right) & 1 \end{bmatrix} \begin{bmatrix} d \\ q \\ 0 \end{bmatrix} \tag{3}$$

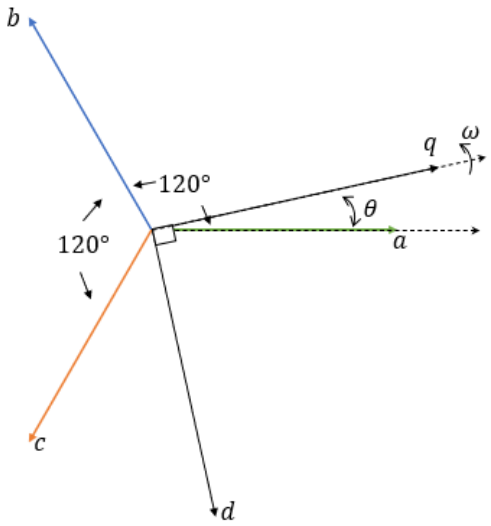

Figure 7- Park transform a-axis align to q-axis

2.2.4.2 Clarke to park transform

Another approach to transferring between reference frames is the alpha-beta zero to direct-quadrant-zero. This method refers to transforming the stationary $\alpha\beta 0$ to $dq0$ rotating reference frame. In other words, it transfers the time variant- to time invariant states with the angle θ [19].

$$T_{C-P} = \begin{bmatrix} d \\ q \\ 0 \end{bmatrix} = \begin{bmatrix} \sin(\theta) & -\cos(\theta) & 0 \\ \cos(\theta) & \sin(\theta) & 0 \\ 0 & 0 & 1 \end{bmatrix} \begin{bmatrix} \alpha \\ \beta \\ 0 \end{bmatrix} \tag{4}$$

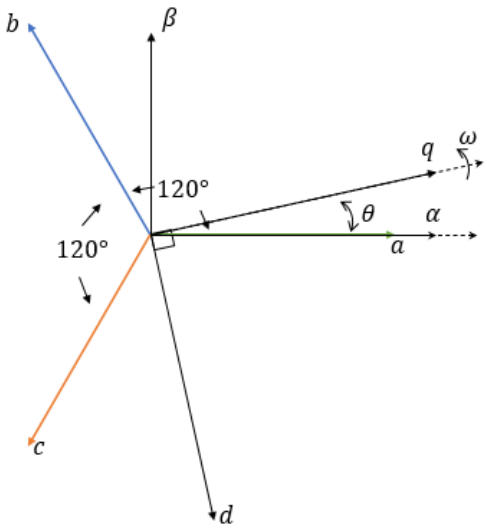

Figure 8 - clarke to park transform

2.3 Battery energy storage system

By deploying battery energy storage systems in weak grids, grid operators and utilities can enhance the grid's reliability, stability, and overall performance. The problem can be addressed with regulating voltage and frequency, enhances power quality, provides backup power, and augment the stability in integration of renewable energy sources [20].

2.4 Software

2.4.1 MATLAB/Simulink

Simulink allows users to build models using a block diagram approach, where each block represents a system component or mathematical operation. These blocks can create complex systems, and users can define inputs, outputs, and parameters to simulate and analyze the behavior of systems. Simulink provides a wide range of built-in blocks, including sources, sinks, linear and nonlinear functions, mathematical operators, and more. It also supports the creation of custom blocks using MATLAB code or other programming languages [21].

2.4.2 Opal-RT

RT-LAB is an industrial-grade software package which can be used for real-time simulations of mathematical block diagrams developed for electrical circuit, control circuit and power systems. To implement any Simulink model in RT-LAB, it is necessary to make certain modifications for transferring the model into the RT-LAB simulation environment. Users must restructure the block diagrams by organizing the models into certain subsystems and integrating OpComm communication blocks between them. Hereby the RT-Lab can run simulation based upon MATLAB/Simulink models in real-time without changing the models behavior [22].

The structure of the subsystems that the model has be divided into is based upon what the functionality is. The console system which the user interacts with under simulations is the system with blocks related to acquiring and viewing data, this can be scopes and manual switches. There can be only one of these in the whole system. The computational elements in the system can be put into either slave or master subsystems. The difference is that the master needs to exist in the system to work and there can only be one, like the console subsystem. Slave subsystems can split up elements in the model, these will use one core of the CPU each. This can make the execution of the model much faster depending on how much computations

there is in the model [23], [24]. The OpComm block is used for communication link between the subsystems, and in order for the RT-Lab OpComm blocks to work in the RT-Labs software, the model has to be running in discrete time and fixed step solver to work properly.

In this thesis a OP4510 which is a FPGA board shown in [fig under] is used with the software provided by RT-Lab to run real-time simulations. The Simulink model's supporting files and test cases are imported into RT-LAB software edited, built, and then compiled, whereby each component of the model is converted into executable C codes. Once the compilation process is successful, the compiled model is loaded onto the target system that is available. The target system handles the model initialization and synchronization, where communication links are established, and then the run-time console becomes active. With the model execution, the simulation begins, and the signals generated during the simulation can be viewed in the active console which is loaded. The results can also be stored in the OpWriteFile block in RT-LAB libraries for further analyses after the execution [23].

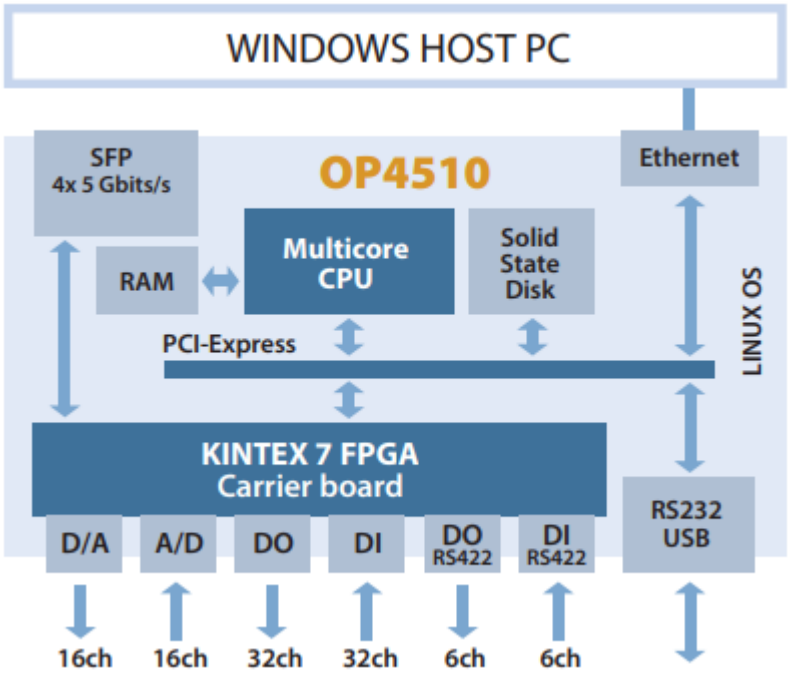

Figure 9 - OP4510 [*25*].

3 Grid-forming converters topology

Grid-following converters have been the most common way of implementing converter-based sources to the grid. Grid-following converters are designed to inject current into the grid while following the voltage of the grid as reference. This means that Grid-following converters require to be synchronized to the grid by using a phase locked loop which measures the voltage angle of the grid. In this case the Grid-following converter locks on the gird and injects active or reactive power according to defined setpoints [26], [27]. Phase locked loop is not suitable due to the impact of grid stability [28]. In other words, they do not follow the grid frequency and lack the possibility to actively control it.

Unlike grid following converters, a more promising solution is Grid-forming converters due to its behavior is more similar to a synchronous machine. Grid-forming converters are designed to actively control the voltage and frequency of the grid. It possesses the ability to restart the grid independently [29]. In other words, they do not need to be synchronized to the grid before operating. This makes them particularly useful in island operation and in situations where the grid is weak or unstable such as problems associated with low inertia. In this practically manner they can help to stabilize the voltage and frequency of the grid, and prevent blackouts or other disruptions. There are several different solutions to grid-forming converters which are based upon the synchronous generator model and frequency response [30].

In recent years, various grid-forming control strategies have been proposed, including droop control which is based on the speed droop mechanism of Synchronous Machines and is widely accepted as a baseline solution. Building on this, Virtual Synchronous Machines strategies have been developed to emulate Synchronous Machines dynamics and control. Additionally, matching control strategies have been proposed that take advantage of the structural similarities between converters and Synchronous Machines and match their dynamic behavior. In contrast to these approaches, Virtual Oscillator Control is a Grid-forming control strategy that utilizes Grid-Forming Converters to replicate the synchronizing behavior of Liénard-type oscillators [31], enabling the possibility for global synchronization of a converter-based power system. Nonetheless, Virtual Oscillator Control has a drawback, it does not allow for the specification of nominal power injection. This limitation is addressed by dispatchable Virtual Oscillator Control that ensures synchronization to a prespecified operating point which satisfies the ac power flow equations [32].

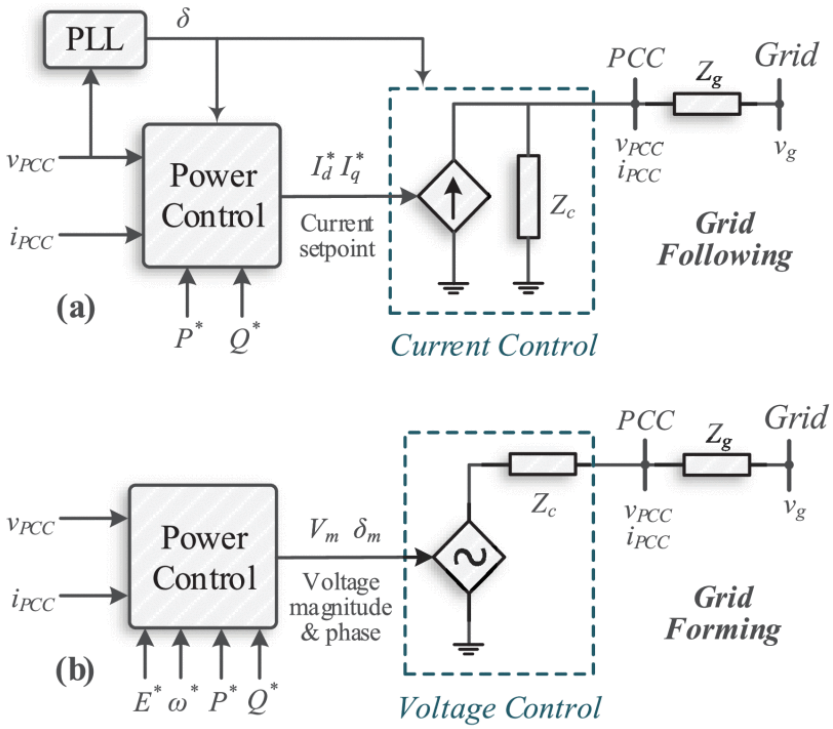

Figure 10 - GFL vs GFM

3.1 Synchronous machine

Since the grid-forming converters is based upon the behavior of the synchronous machine, it is suggested an eight-order balanced, symmetrical, three-phase synchronous machine with a field winding and three damper windings on the rotor with two poles shown in Figure 11 [33].

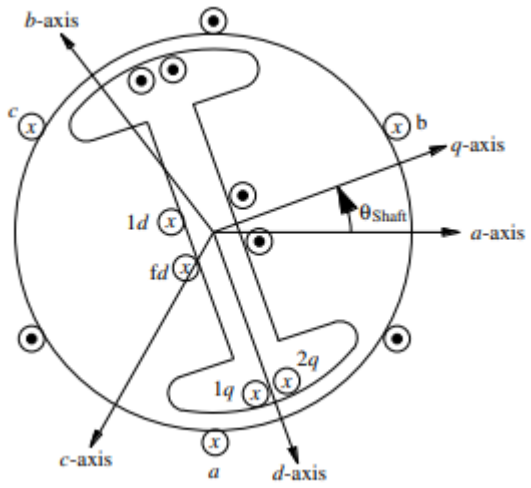

Figure 11 - two pole salient pole machine [*33*].

$$\frac{d\theta_{shaft}}{dt} = \frac{2}{P}\omega \tag{5}$$

$$J\frac{2}{P}\frac{d\omega}{dt} = T_m - T_e - T_f \tag{6}$$

$$\frac{d\lambda_{fd}}{dt} = v_{fd} - i_{fd}r_{fd}$$

$$\frac{d\lambda_a}{dt} = v_a - i_a r_s, \qquad \frac{d\lambda_b}{dt} = v_b - i_b r_s, \qquad \frac{d\lambda_c}{dt} = v_c - i_c r_s \tag{7}$$

$$\frac{d\lambda_{1d}}{dt} = v_{1d} - i_{1d}r_{1d}, \qquad \frac{d\lambda_{1q}}{dt} = v_{1q} - i_{1q}r_{1q}, \qquad \frac{d\lambda_{2q}}{dt} = v_{2q} - i_{2q}r_{2q} \tag{8}$$

Park`s transform can be used to convert the sinusoidal steady state of balanced symmetrical machines power variant terms into constant states. By transforming equations [5]-[8] with equations [2]-[3] the $dq0$ coordinates and considering a two-pole machine the results becomes (note that $\theta_{shaft} = \theta$) [33]:

$$\frac{d\theta_{shaft}}{dt} = \omega \tag{9}$$

$$J\frac{d\omega}{dt} = T_m - T_e - T_f \tag{10}$$

$$\frac{d\lambda_{fd}}{dt} = v_{fd} - i_{fd}r_{fd} \tag{11}$$

$$\frac{d\lambda_d}{dt} = v_d - i_d r_s + \lambda_d\omega, \qquad \frac{d\lambda_q}{dt} = v_q - i_q r_s + \lambda_d\omega, \qquad \frac{d\lambda_0}{dt} = v_0 - i_0 r_s \tag{12}$$

$$\frac{d\lambda_{1d}}{dt} = v_{1d} - i_{1d}r_{1d}, \qquad \frac{d\lambda_{1q}}{dt} = v_{1q} - i_{1q}r_{1q}, \qquad \frac{d\lambda_{2q}}{dt} = v_{2q} - i_{2q}r_{2q} \tag{13}$$

Where ω is the rotor angular velocity and becomes as extra term after transformation, θ_{shaft} the rotor angle and is the same as θ from Figure 7. J is the inertia constant, and T_m, T_e, T_f is representing the mechanical torque applied to the shaft, torque of electrical origin, and friction windage torque. Moreover r_s and r_{fd} is the winding resistance in the stator and field, the d-axis field winding flux, voltage and current is represented as λ_{fd}, v_{fd} and i_{fd}, and $\lambda_{d,q,0}$ is

the winding fluxes, $v_{d,q,0}$ the voltages, and $i_{d,q,0}$ the currents in the stator referring to the $dq0$ - coordinate with the angle θ_{shaft}. Furthermore $\lambda_{1d,1q,2q}$, $v_{1d,1q,2q}$ and $i_{1d,1q,2q}$ represents the linkage fluxes, voltages, and currents in the damper windings, and $r_{1d,1q,2q}$ is the damper windings resistances in the rotor [32], [33].

3.2 Droop control

The droop control characteristic is used to regulate the output voltage and frequency of a power inverter in a parallel-connected system without the need of communication between them [34]. Each inverter in the system is assigned a specific droop coefficient, which determines the rate at which the output frequency is reduced as the output active power increases. Similarly, a droop in the voltage with respect to the reactive power. This ensures that the load is shared evenly between all the inverters in the system, such that the grid remains stable. Droop is a very common way to control active power and frequency [35].

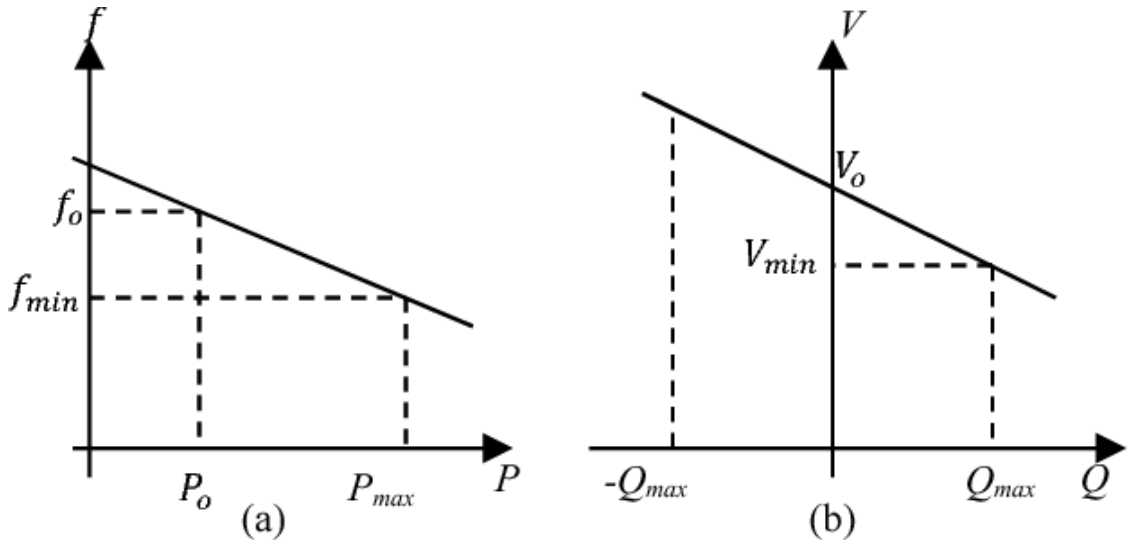

Figure 12 – Convential droop characteristics [36].

3.2.1 Droop model

Droop control shares similarities with the speed droop characteristic of the synchronous machine governor and compensates for deviations in power injection from p^* and frequency deviations from ω^*. The droop gain is denoted by d_ω. To emulate the Automatic Voltage Regulations functionality in synchronous machines, a proportional integral controller is utilized to address the output voltage error [32].

$$\frac{d\theta}{dt} = \omega \tag{14}$$

$$\omega = \omega^* + d_\omega(p^* - p) \tag{15}$$

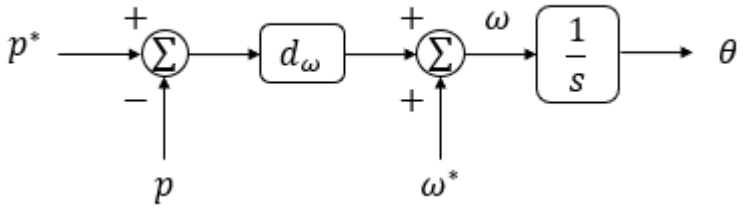

Figure 13 - Droop control P-ω

To determine the direct axis reference v_d^* for the underlying voltage loop, the reference and measured voltage magnitude form the voltage source converter are represented by v_{ref} and $\|v_{dq}\|$, respectively. It should be noted that $\|v_{dq}\|$ is transformed from abc- to $dq0$ - reference frame, v_q^* is set to 0 and the reactive power injection varies to ensure precise voltage regulation. This will give a result for the v_d^* to become v_{dq0}^* which is injected into the AC voltage control loops in Figure 19 [32].

$$v_d^* = k_p\left(v_{ref} - \|v_{dq}\|\right) + k_i \int_0^t \left(v_{ref} - \|v_{dq}(\tau)\|\right) d\tau \tag{16}$$

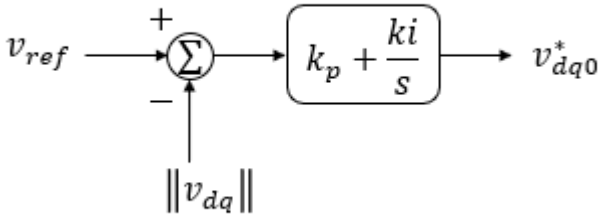

Figure 14 - droop control Q-V

3.3 Virtual synchronous machine

The Virtual Synchronous Machine can be chosen as a synchronverter, the synchronverter has a unique characteristic in that it models all the parameters of synchronous generator within it. Therefore, any control strategies that have been developed for synchronous generator can be applied to the synchronverter. Additionally, it has the same dynamics as synchronous

generator and can function as a synchronous motor, which distinguishes it from other machine-emulating techniques. Unlike other methods, the synchronverter can operate in Grid-forming converter and Grid-following converter mode without adhering to a specific voltage or current reference [34].

One of the key advantages of the synchronverter over the original synchronous generator is the benefit of readily tuning the parameters such as inertia, damping, field inductance, and mutual inductances [37].

3.3.1 Virtual synchronous machine model

For the virtual synchronous machine, a synchronverters frequency dynamics is evaluated as follow.

$$\frac{d\theta}{dt} = \omega \tag{17}$$

$$J_r \frac{d\omega}{dt} = \frac{1}{\omega^*}(p^* - p) + D_p(\omega^* - \omega) \tag{18}$$

Where $D_p(\omega^* - \omega)$ is called virtual damping, which is derived from the speed droop response of a synchronous machine. However, the speed-dependent term in equation[wr] does not have an exact analog in a synchronous machine. This is because the response of the damper windings and turbine governor in a synchronous machine operates at different timescales and does not act relative to the nominal frequency. In contrast, the speed-dependent term in equation [18] provides both damping and steady-state behavior that is equivalent to synchronous machine turbine governor droop with respect to the nominal frequency [32]. The J_r term is the virtual inertia constant, and when $\lim_{n\to 0} J_r/D_p$ the equation [18] reduces to the droop control equation [15].

The equations for the output voltages are questionable since it is represented with two times the angular velocity of the synchronverter. Other research papers do not include it [37], [38] and it is neither represented in the Simulink control scheme. Hereby the three-phase induced voltage by the virtual synchronous machine is given by:

$$\begin{bmatrix} v_a^* \\ v_b^* \\ v_c^* \end{bmatrix} = \frac{d\theta}{dt} M_f i_f \begin{bmatrix} \sin(\theta) \\ \sin\left(\theta - \frac{2\pi}{3}\right) \\ \sin\left(\theta + \frac{2\pi}{3}\right) \end{bmatrix} \tag{19}$$

$$i_f = \frac{k_p}{M_f}\left(v_{ref} - \|v_{dq}\|\right) + \frac{k_i}{M_f}\int_0^t \left(v_{ref} - \|v_{dq}(\tau)\|\right) d\tau \tag{20}$$

By transforming the time-varying phasors $[v_a^* \ v_b^* \ v_c^*]^T$ to $dq0$ – coordinates it will be in the same reference frame as the low-level cascaded control system in Figure 19

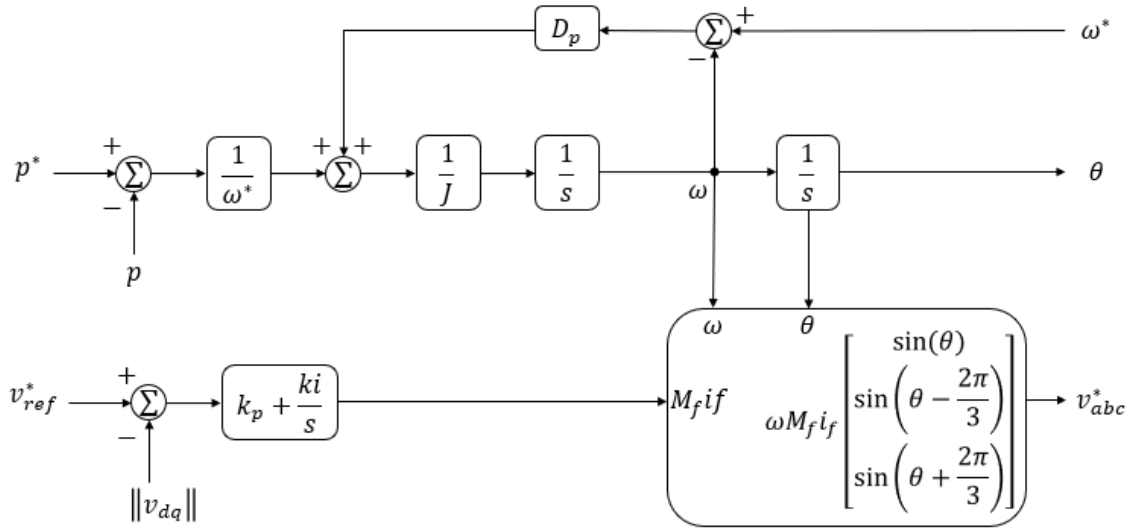

Figure 15 – block diagram of virtual synchronous machine model

3.4 Matching control

The Synchronous Generator and inverter model have structural similarities that enable the implementation of a matching control topology. This topology controls the DC link in a manner that is similar to controlling a mechanical rotor. However, matching control differs from the synchronverter in that it employs a DC link to drive the harmonic frequency oscillator instead of using a Synchronous Generator model. A controller drives the inverter modulation based on the internal oscillator model embedded within it. The DC link voltage is utilized to monitor power balance, and active power tracking is achieved by controlling the DC current, resulting in oscillator frequency and voltage control. As only DC-side measurements are utilized in matching control, there are no processing delays. In other words, Matching control can be referred as the duality of the DC voltage of the converter and the machines angular velocity. The DC-Link capacitor voltage is used for controlling the frequency of the converter bridge, due to the DC-link capacitor is considered as a storage device similar to the concept of inertia [30].

3.4.1 Matching control model

The angle dynamics of matching control is represented by.

$$\frac{d\theta}{dt} = \frac{\omega^*}{v_{dc}^*} v_{dc} \tag{21}$$

The ac voltage magnitude is controlled through the modulation magnitude by recalling equation [16] and referring it as μ. Then the reference voltage for the voltage controller in $\alpha\beta$ – coordinates is given by:

$$\mu = k_p\left(v_{ref} - \|v_{dq}\|\right) + k_i \int_0^t \left(v_{ref} - \|v_{dq}(\tau)\|\right) d\tau \tag{22}$$

$$\begin{bmatrix} v_\alpha^* \\ v_\beta^* \end{bmatrix} = \mu \begin{bmatrix} -\sin(\theta) \\ \cos(\theta) \end{bmatrix} \tag{23}$$

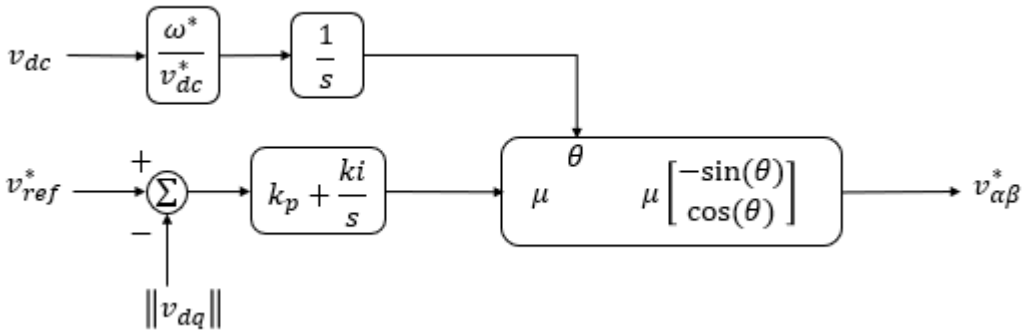

Figure 16 - block diagram of matching control model.

By alpha beta zero to $dq0$ with equation [4], the desired reference frame is obtained like previous discussed for other control methods.

3.5 Dispatchable virtual oscillator control

Proposed solutions based on Virtual Oscillator Control have shown improved dynamic performance and maintained an embedded droop control law close to steady-state. This implies superior voltage regulation performance compared to standard droop control, while also retaining load-sharing capabilities. Furthermore, the ease of synchronization makes Virtual Oscillator Control a promising option for microgrids. However, it remains unclear how to dispatch Virtual Oscillator Control in such systems. For example, how to reconfigure the inverters power injections as they have no programmable power set-points.

Dispatchable Virtual Oscillator Control is a control strategy designed to achieve synchronization of an inverter-dominant grid, while maintaining a level of control on the power injections and voltage level of each inverter which can be set by its user. When applying Dispatchable Virtual Oscillator Control, each inverter monitors its output current and by using a Pulse Width Modulation strategy, it can regulate the terminal voltage vector at the output bus by [39].

3.5.1 Dispatchable virtual oscillator control model

The dynamics of the dispatchable virtual oscillator control in $\alpha\beta$ – coordinates

$$\frac{dv^*_{\alpha\beta}}{dt} = \omega^* \mathcal{J} v^*_{\alpha\beta} + \eta(\mathcal{K} v^*_{\alpha\beta} - \mathcal{R}(\varkappa) i_{\alpha\beta} + \alpha\phi\left(v^*_{\alpha\beta}\right) v^*_{\alpha\beta} \tag{24}$$

$$\mathcal{R}(\varkappa) = \begin{bmatrix} \cos(\varkappa) & -\sin(\varkappa) \\ \sin(\varkappa) & \cos(\varkappa) \end{bmatrix} \tag{25}$$

is a 2D rotaion matrix, $\mathcal{J} = \mathcal{R}(\pi/2)$ which gives:

$$\mathcal{R}\left(\frac{\pi}{2}\right) = \begin{bmatrix} \cos\left(\frac{\pi}{2}\right) & -\sin\left(\frac{\pi}{2}\right) \\ \sin\left(\frac{\pi}{2}\right) & \cos\left(\frac{\pi}{2}\right) \end{bmatrix} = \begin{bmatrix} 0 & -1 \\ 1 & 0 \end{bmatrix} = \mathcal{J} \tag{26}$$

$$\mathcal{K} := \frac{1}{v^2_{ref}} \mathcal{R}(\varkappa) \begin{bmatrix} p^* & q^* \\ -q^* & p^* \end{bmatrix}, \qquad \phi\left(v^*_{\alpha\beta}\right) := \frac{v^2_{ref} - \left\| v^*_{\alpha\beta} \right\|^2}{v^2_{ref}} \tag{27}$$

α and η represents the postive control gains, $\varkappa$ is the design paramerter and ranges from $0 < \varkappa < \pi$ where 0 refers to resitive lines and $\pi/2$ to inductive lines. The p^*, $q^*$and v^* represents the active power, reactive power and voltage magnitude set-points, when $\mathcal{K} v^*_{\alpha\beta} - \mathcal{R}(\varkappa) i_{\alpha\beta} = 0$ and $\left\| v^*_{\alpha\beta} \right\| = v_{ref}$ the dynamics in equation [24] reduces to a harmonic oscillator [39]. Moreover the research indicates that if all inverters in the grid comply with the AC power-flow equations and if additional technical requirements is met, the inverter-based grid achieves (almost) global asymptotic stability refered to the desired power-flows. This implies that the inverters synchronize and reach the desired set-points regardless of the initial conditions. Additionally, the dipsatchable virtual oscillator control behave with droop-like chractersitcs when the set-points deviate from the power flow equations [39]. By rewriting

equation [24] to the polar coordinates and with inductive lines, the droop characterstics of the dVOC becomes:

$$\frac{d\theta}{dt} = \omega^* + \eta\left(\frac{p^*}{v_{ref}^2} - \frac{p}{\left\|v_{dq}^*\right\|^2}\right) \tag{28}$$

$$\frac{d\left\|v_{dq}^*\right\|}{dt} = \eta\left(\frac{q^*}{v_{ref}^2} - \frac{q}{\left\|v_{dq}^*\right\|^2}\right) + \frac{\eta\alpha}{v_{ref}^2}\left(v_{ref}^2 - \left\|v_{dq}^*\right\|^2\right)v_{dq}^* \tag{29}$$

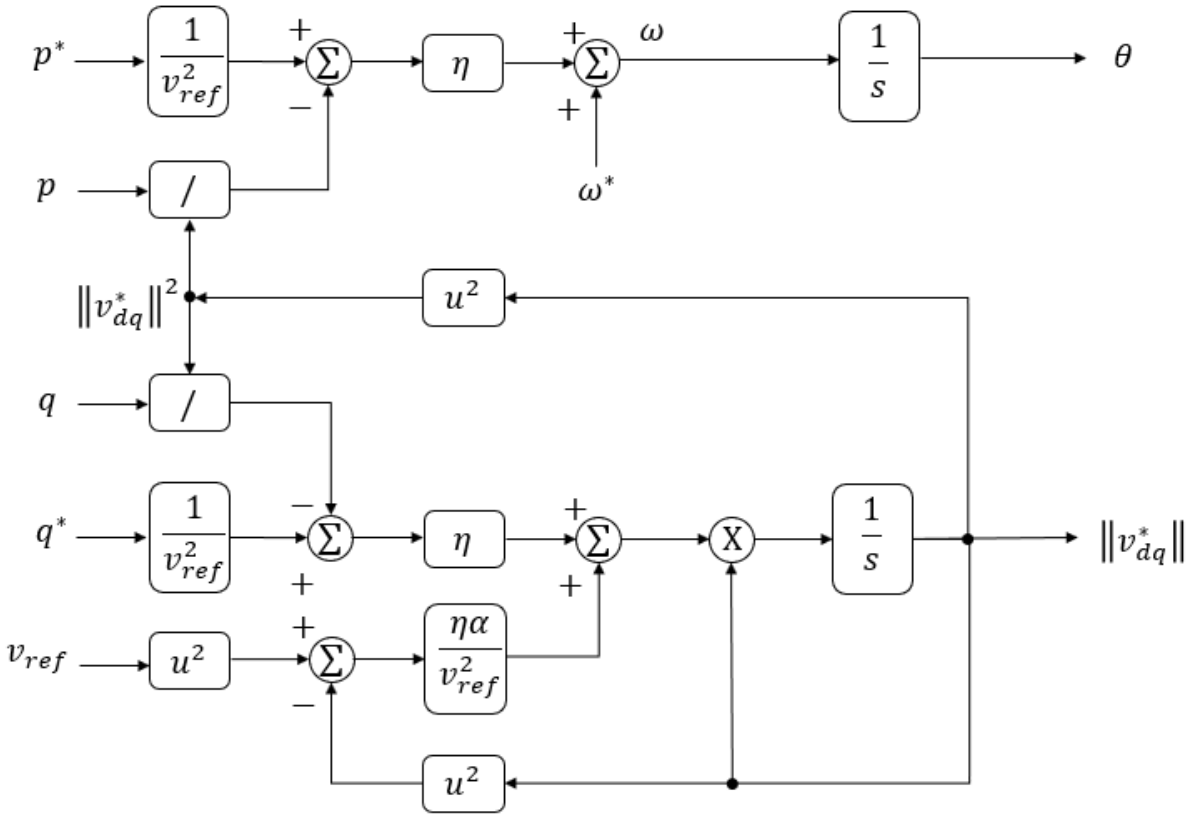

Figure 17 - Block diagram of dispatchable virtual oscillator control

3.6 Voltage source converter

A voltage source converter is an electronic device used in power electronics to convert electrical power from one form to another. Voltage source converter is suitable for grid-forming converter due the ability to convert electrical power from one voltage level to another, and can also convert AC power to DC power, or vice versa.

Converter model in $\alpha\beta$ – coordinates illustrated in Figure 18 given by

$$C_{dc}\frac{dv_{dc}}{dt} = i_{dc} - G_{dc}v_{dc} - ix \tag{30}$$

$$L_{AC}\frac{di_{s,\alpha\beta}}{dt} = v_{\alpha\beta} - R_{AC}i_{s,\alpha\beta} - v_{\alpha\beta} \tag{31}$$

$$C\frac{dv_{\alpha\beta}}{dt} = i_{s,\alpha\beta} - i_{\alpha\beta} \tag{32}$$

In the model it is considered that the DC-supply current i_{dc} and the AC-grid voltage $v_{s,\alpha\beta}$ is external inputs, hereby the model of the VSC is based upon certain network dynamics shown under. The C_{dc} is dc-link capacitance, G_{dc} block is the parallel conductance modeling (switching) losses in the dc link, while R_{AC} , L_{AC} and C is the filters for the VSC. Further the v_{dc} and i_{dc} represent the voltage and the current flowing out of the controllable DC energy source model in Figure 18. $m_{\alpha\beta}$ is the modulation signal from the full-bridge average switching stage model. $i_x = \frac{1}{2}m_{\alpha\beta}^T i_{s,\alpha\beta}$ represent the net dc current delivered to the switching stage to the converter, while $i_{s,\alpha\beta}$ and $v_{s,\alpha\beta} = \frac{1}{2}m_{\alpha\beta}v_{dc}$ are the AC side switching current and voltage from the converter before the filter, and after the filter $i_{\alpha\beta}$ and $v_{\alpha\beta}$ are the output current and voltages to the AC grid [32].

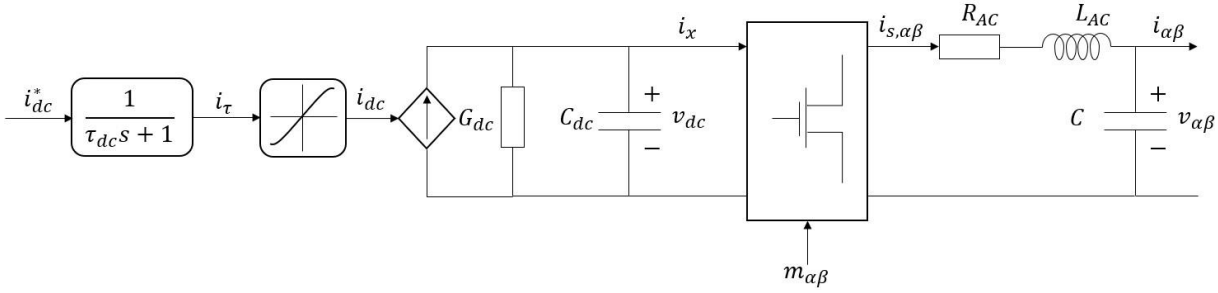

Figure 18 - DC energy source for Voltage Source Converters

Looking into the response time for the first order system to calculate and make a realistic model of the DC energy source.

$$\tau_{dc}i_\tau = i_{dc}^* - i_\tau \tag{33}$$

Where i_{dc}^* is the DC current reference injected by the set values of power and voltage references. τ_{dc} is the time constant in the dc-link, and the saturation limits for controlling the current limitation is modelled in such a way that it does not get an over current [32].

$$i_{dc} = sat(i_\tau, i_{max}^{dc}) = \begin{cases} i_\tau, & if\ |i_\tau| < |i_{max}^{dc}| \\ sgn(i_\tau) i_{max}^{dc}, & if\ |i_\tau| \geq |i_{max}^{dc}| \end{cases} \quad (34)$$

Where the i_{max}^{dc} from equation[above] is the maximum dc source current. It is also in the model implemented and considered the dc-losses for the limits [32].

3.6.1 DC voltage control

The controllable dc source in equation [33] the current reference i_{dc}^* is given by the dc voltage control and feed- forward terms based on the nominal ac power injection p^* and the filter losses.

$$i_{dc}^* = k_{dc}(v_{dc}^* - v_{dc}) + \frac{p^*}{v_{dc}^*} + \left(G_{dc} v_{dc} + \frac{v_{dc} i_x - p}{v_{dc}^*}\right) \quad (35)$$

In equation [above], $v_{dc} i_x$ represents the DC power flowing into the switches, while p is the AC power injected into the grid. The final term on the right side of the equation is a feedforward power control that compensates for filter losses. The compensation is necessary to ensure exact tracking of the power reference by matching control, this improves the dc voltage regulation for all the control strategies suggested in this paper [32].

3.6.2 Low-level cascaded control design

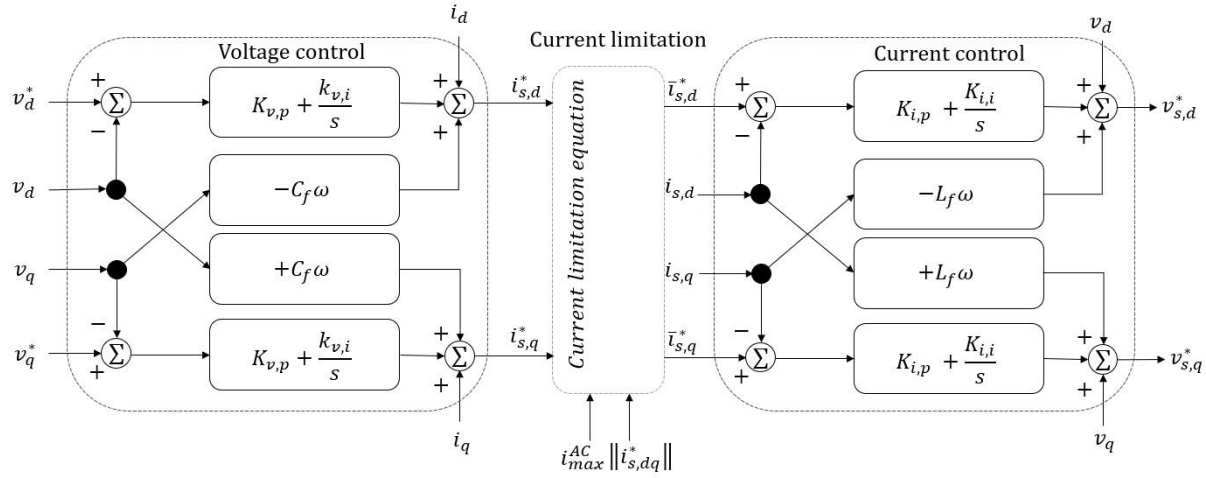

Figure 19 - The control loop for Voltage Source Converter

3.6.2.1 AC voltage control

The chosen grid-forming model provides the reference voltage with its angle and magnitude by measuring the voltage at the AC side of the converter and feed it through a park transform

to get $dq0$ reference frame, resulting in v_{abc} to v_{dq}. In order to get the reference current $i^*_{s,dq}$ for the switching node current $i_{s,dq}$, the voltage tracking error $v^*_{dq} - v_{dq}$ needs to be applied. The equations for each axis in Figure 19 can be described as follows.

$$\frac{d\phi_{v,d}}{dt} = v^*_d - v_d \ , \qquad \frac{d\phi_{v,q}}{dt} = v^*_q - v_q \tag{36}$$

$$i^*_{s,d} = i_d - C_f \omega v_q + k_{v,p}(v^*_d - v_d) + \ k_{v,i}\phi_{v,d} \tag{37}$$

$$i^*_{s,q} = i_q + C_f \omega v_d + k_{v,p}\left(v^*_q - v_q\right) + \ k\phi_{v,q} \tag{38}$$

The measured currents $i_{d,q}$ and the filters is the feed forward terms, while the two last terms for the proportional-integral controller, to get the reference current at the time domain [32], [40].

3.6.2.2 AC current limitation

The stability margins and dynamics of grid-forming power converters can be significantly affected by restricting the ac current. Developing a reliable strategy that can handle load-induced overcurrent and grid faults remains an unresolved research challenge. Due to the complexity of current limitations strategies as they need careful tuning of the controllers, it is suggested a straightforward ac current limitation strategy [32].

for protection of the converter, it must be implemented current restriction at the AC side. A proposed solution is to scale down the reference current i^{AC}_{max} by these settings.

$$\bar{\imath}^*_{s,dq} = \begin{cases} i^*_{s,dq}, & if \ \left\| i_{s,dq} \right\| \le i^{AC}_{max} \\ \dfrac{i^{AC}_{max}}{\left\| i^*_{s,dq} \right\|} i^*_{s,dq}, & if \ \left\| i_{s,dq} \right\| > i^{AC}_{max} \end{cases} \tag{39}$$

Where $\bar{\imath}^*_{s,dq}$ denotes the limited reference current and preserves the direction of $i^*_{s,dq}$.

3.6.2.3 AC current control

On the right side of Figure 19 shows the current controller structure. The same control strategy for the voltage control is applied, here is the output filter inductor current control achieved with a standard proportional integral controller. $k_{i,p}$ and $k_{i,i}$ represents the proportional and integral gains, the current has a reference frame that is used for practical

similarities. The equations for the gains and voltages represented in their respective axis for the reference frame [32].

$$\frac{d\gamma_{i,d}}{dt} = \bar{\imath}^*_{s,d} - i_{s,d} \ , \qquad \frac{d\gamma_{i,q}}{dt} = \bar{\imath}^*_{s,q} - i_{s,q} \tag{40}$$

$$v^*_{s,d} = v_d - L_f \omega i_{s,q} + k_{i,p}\left(\bar{\imath}^*_{s,d} - i_{s,d}\right) + \ k_{i,i}\gamma_{i,d} \tag{41}$$

$$v^*_{s,q} = v_q + L_f \omega i_{s,d} + k\left(\bar{\imath}^*_{s,q} - i_{s,q}\right) + \ k_{i,i}\gamma_{i,q} \tag{42}$$

Then for the modulation signal to voltage source converter shown in Figure 20 is given by.

$$m_{\alpha\beta} = \frac{2v^*_{s,\alpha\beta}}{v^*_{dc}} \tag{43}$$

Where the $v^*_{s,\alpha\beta} = v^*_{s,dq}$ in $\alpha\beta$- coordinates and v^*_{dc} is the set reference dc voltage for the converter. The complete model with control loops and voltage source converter in Figure 20. The gain m_{ab} represent the features possessed in $m_{\alpha\beta}$, while k_p ,k_{pref} and $k_{dc,ref}$ referring to the terms in equation [35]

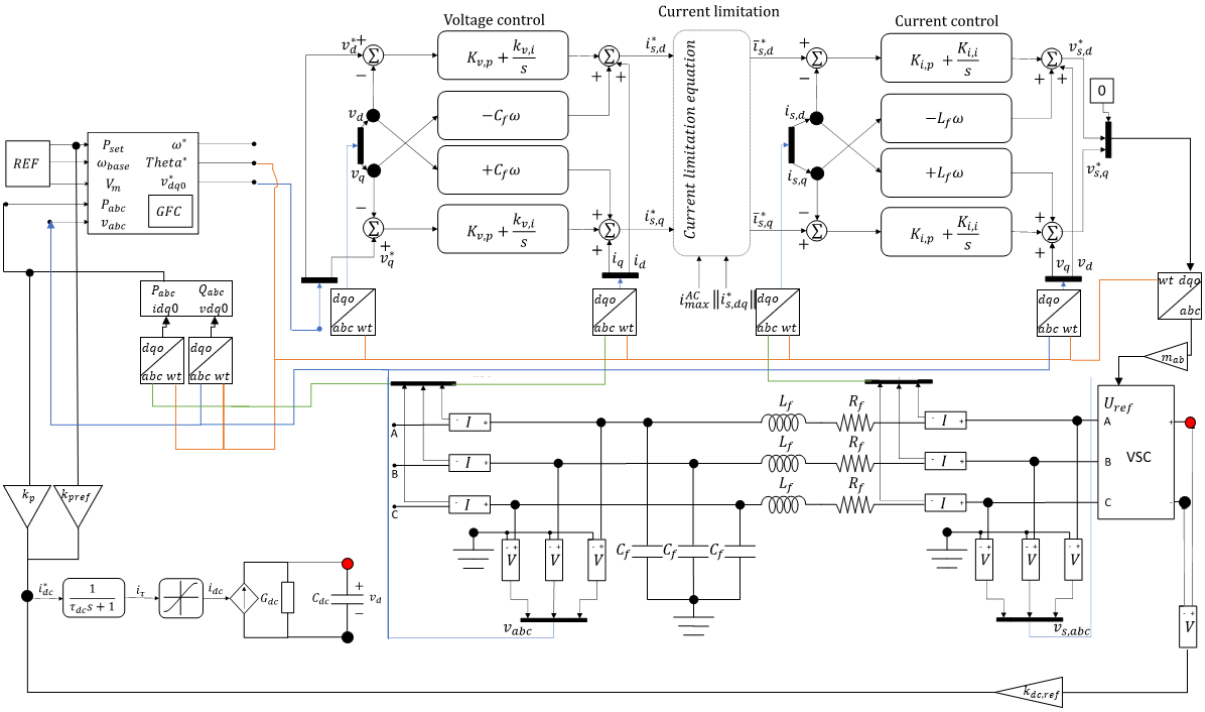

Figure 20 - Voltage source converter with control loops and Grid-forming converter

3.7 Network

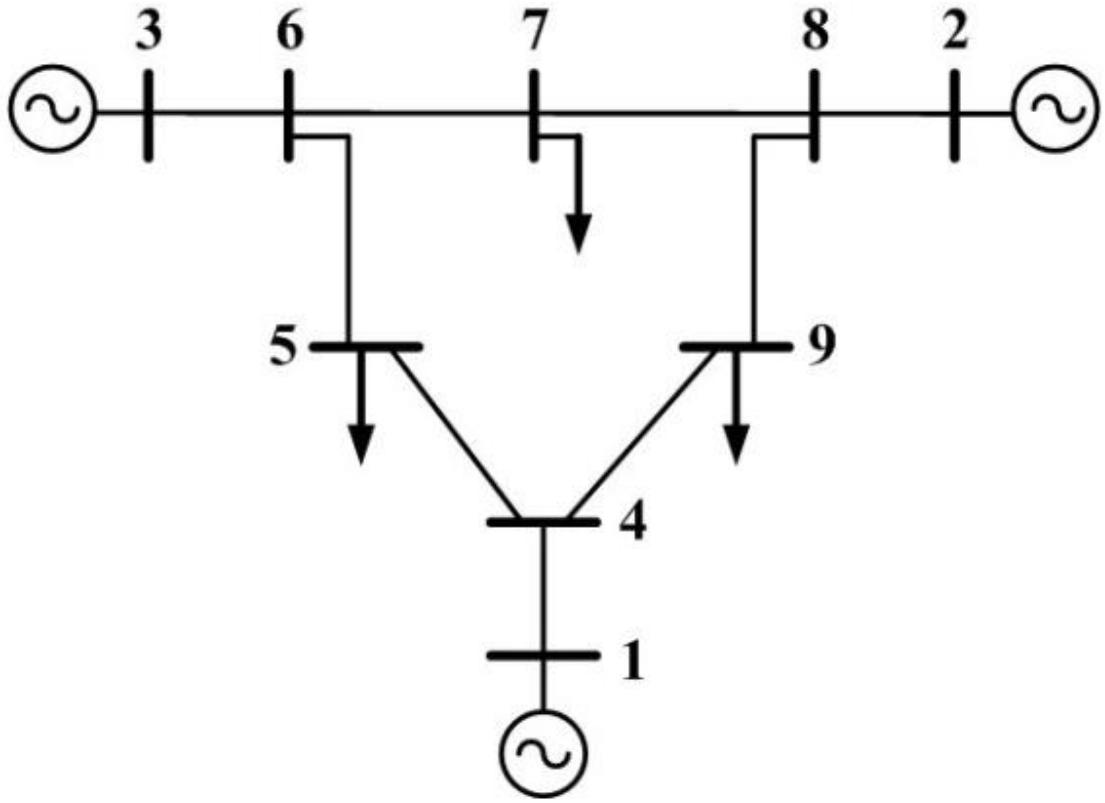

Figure 21 – IEEE nine-bus [41].

Connecting all these different methods of providing power to the grid can be achieved with an nine-bus system for understanding how they will operate under different conditions. The IEEE nine-bus system is a simplified representation of a small power system, and it is used for evaluating power system analysis and for comparing the performance of different control strategies. The system consists of nine buses, three generators and transmission lines between. The transmission lines are represented as impedance values in per unit, and they connect the different buses. The per-unit values are based on the line length, the -resistance, and the -reactance, it also possesses three shunt capacitances. The nine-bus system as a single-line diagram shown in Figure 21, where each bus is represented as a node, and the transmission lines are represented as branches connecting the nodes.

The nine-bus test system can be used for various power system analysis techniques, such as load flow, transient stability, and fault analysis. The results obtained from the analysis can be used to evaluate the system's performance, such as voltage stability, frequency behavior, power sharing and fault response. This makes it suitable for testing grid-forming converters topology [42].

4 Model

4.1 Initial model

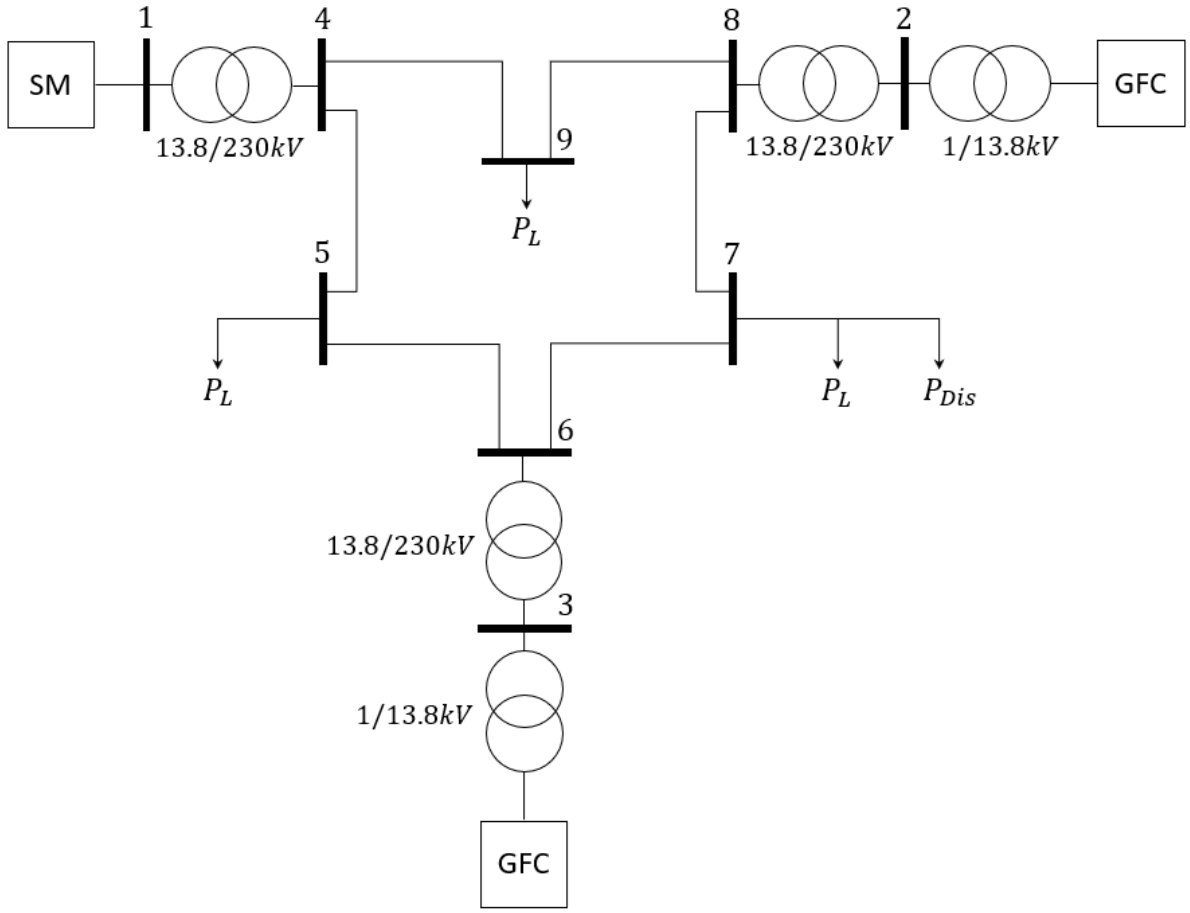

Figure 22 - Network of model

The decision upon building the models from research paper and dynamic modeling where concerned, but building such a big and complex system within a short amount of time would take too much time. Therefore, a decision was made to take advantage of premade models from A. Tayebi, which included four grid-forming converters. These particular models were chosen because they have already been implemented in a nine-bus system.

The model consists of grid-forming converters that are made up of 200 commercial converter modules rated at 500 kVA each. The total capacity of the these are rated at 100 MVA, which is the same as the synchronous machine rating in the models. Each converter module is connected to a medium level high voltage line through a transformer (see Figure 22) and with 100 commercial transformers rated at 1.6 MVA are connected in parallel. The grid itself consist of real and reactive elements to imitate realistic grids, and parameters for the system can be found in table 1 in [32].

All the loads in the nine-bus system only consume real power and have a constant impedance, it consists of three loads, but an additional load representing a disturbance has been added to the setup. The Simulink RLC load block does not allow for modifications to the impedance or power rating during a simulation, but this is not a concern because all loads, except for the disturbance load, are met with power production. The disturbance load is connected behind a switch, which is preferable because sudden big changes in power demand mimic real-time situations seen as a fault. When power demand slowly changes, the synchronous machine and the dynamics in the grid-forming converters can handle it by adjusting the power input, resulting in less deviation in frequency compared to when a big disturbance occurs.

The synchronous machine is behind a delta star connection. This can be explained with, when a delta is on the primary side you will always achieve magnetomotive force balance. In other words, the current does not flow to neutral like in a star connection. This will make the angle and magnitudes from the synchronous machine precise in terms of feedback. The machine itself is equipped with a governor, a generic power system stabilizer and an excitor.

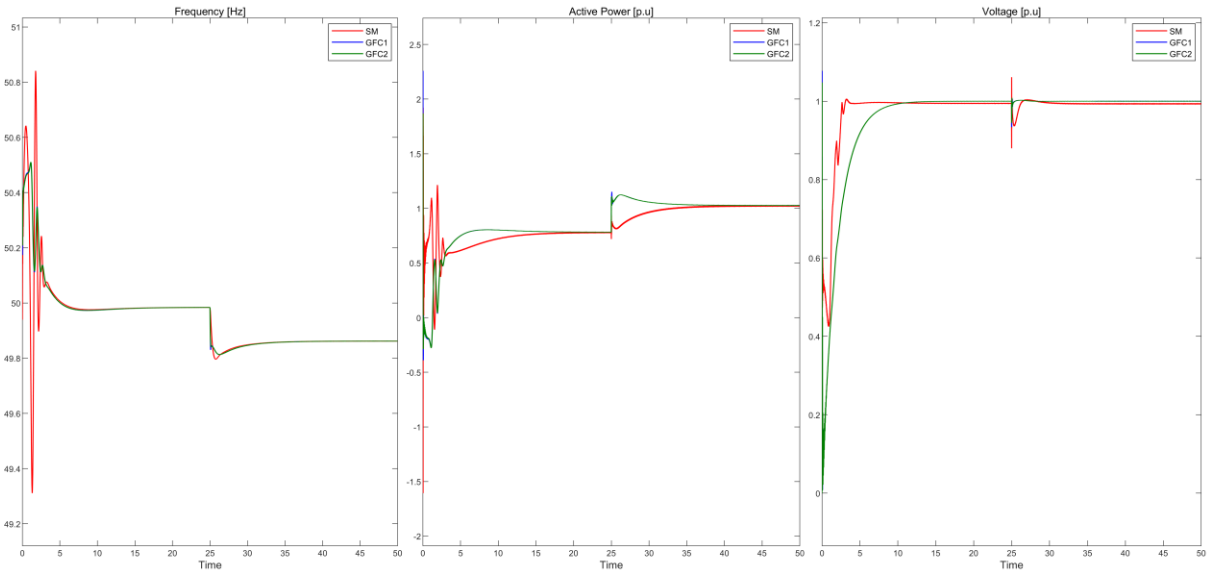

Figure 23 - Responses to the system without changes

Figure 23, only nadir and rate of change of frequency features are employed when the fault occurs. It is clear that the grid-forming converters dynamics are faster compared to the synchronous machine, as seen in the active power deviations.

4.1.1 Governor

The governor is modeled by proportional speed droop and turbine by a first order transfer function.

$$p = p^* + d_p(\omega^* - \omega) \tag{44}$$

$$\tau_g \dot{p_\tau} = p - p_\tau \tag{45}$$

Where p is the output power, p^* the reference power set point. d_p is the droop gain and $\omega^* - \omega$ is the error in rotational speed. p_τ and τ_g is the turbine outpower and time constant, respectively [32]. The figure 24 block diagram is based upon the models for governor derived in [1].

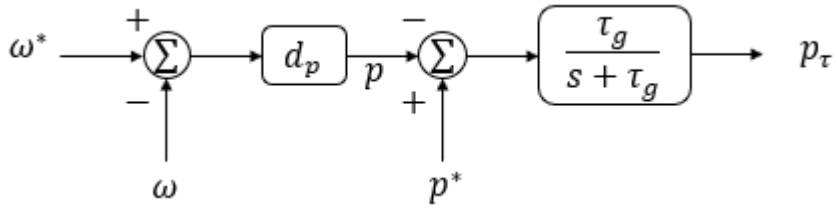

Figure 24 - Block diagram of governor control

4.1.2 Excitor

The exciter in the model is a ST1A excitation system. The model is described in Figure 25 and its ratings in Table 1 [5].

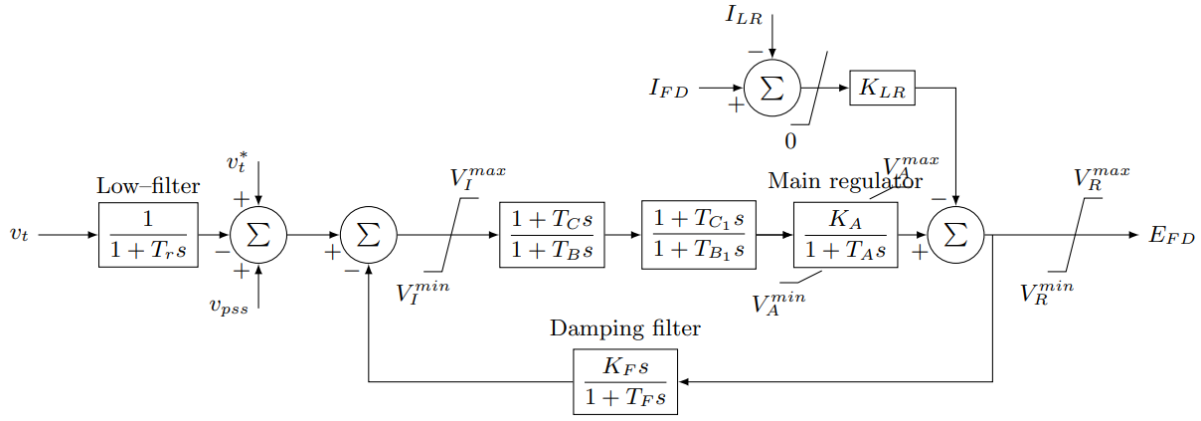

Figure 25 - ST1A Excitation system [43].

Table 1 - Exciter data

Exciter	
Low- pass filter	0.02
Voltage regulator (KA, TA(s))	[210, 0.001]
Voltage regulator input limits (min, max)	[-999, 999]
Voltage regulator internal limits (min, max)	[-999, 999]
Voltage regulator output limits (min, max)	[-6, 6.43]
Damping filter gain and lag time	[0.001, 1]
Transient gain reduction Lead and lag time constants (TB, TC, TB1, TBC1)	[0, 0, 0, 0]

4.1.3 Generic power system stabilizer

The power system stabilizer in the model is damping the rotor oscillations of the synchronous machine by controlling the ST1A excitor. The model is described in Figure 26 and its ratings in Table 2.

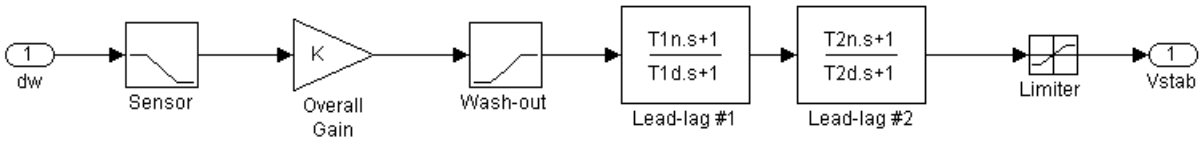

Figure 26 – PSS [44].

Table 2 – Generic power system stabilizer data

Power system stabilizer	
Sensor time constant	0.003
Overall Gain	2.5
Wash-out time constant	2
Lead lag #1 time constant	[0.1, 0.002]
Lead lag #2 time constant	[6, 0.54]
Output limiter	[-0.3, 0.3]

4.2 Control application

The main idea behind this control application is to increase or decrease power into the system in steps over desired time to meet the production and consumption, where the frequency regulations is highly considered. This is achieved with triggers that detects when a load is changing in the bus.

A three phase V-I measurement is used to the detect the power in the bus where predefined load disturbance occurs, this is compared to the set-power to meet the actual demand. Furthermore, the abc to $dq0$ transformation on the measured voltages and currents is applied for getting the reference instantaneous powers. The reactive power output is terminated for the reason of only active power in the loads. In this branch a low pass filter for the measured instantaneous power is employed, this is a filter that attenuates high-frequency components of the signal while allowing low-frequency components to pass through. The first order digital filter smooths out the rapid changes in the signal when using the switches, resulting in making the system response better when simulating.

There are two states for the triggers in the system, 0 and 1. When one of these changes state, an output signal is sent through a Boolean logical operator to set a signal to a reset integrator, this activates the step response of power injections. A truth table of an XNOR logic operator is shown in Table 3 and Figure 27 shows the controller.

Table 3 - Logic table XNOR Operator

A	B	Out
0	1	0
1	1	1
1	0	0
0	0	1

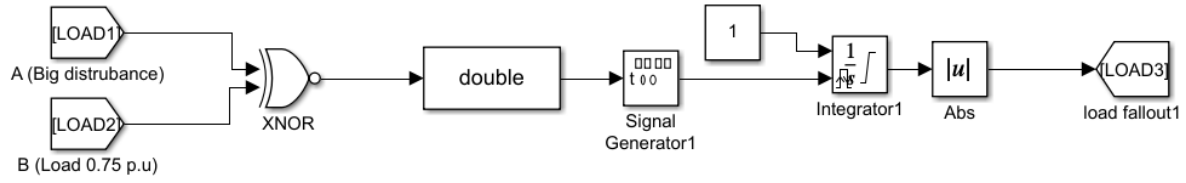

Figure 27 - Control application of the trigger signal.

By Table 3 it is shown that for all the combination a rising or falling edge is achieved based upon only one trigger event a time, which control the reset signal for the integrator in Figure 27.

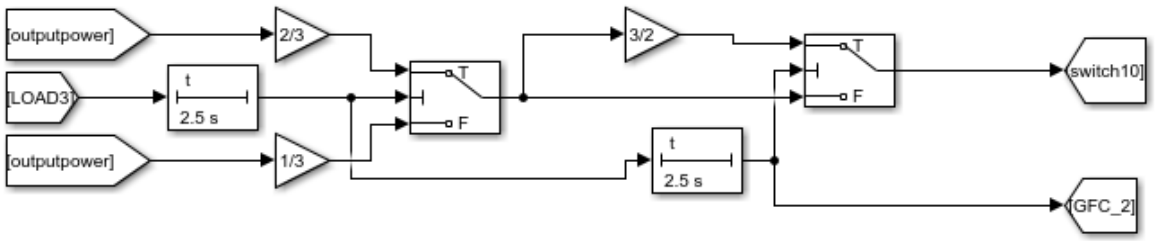

Figure 28 - Timing events for power injections

The idea behind Figure 28 is to inject the power deviation in steps as discussed, first 1/3 of the output power is passed through, then 2/3 and finally the whole signal through the 3/2 gain.

The Goto blocks “switch 10” and “GFC_2” represent the controller signal that is passed through when LOAD_3 is activated and a signal to timing events for the second generator unit, respectively (see Figure 28). After the execution of the timing events, one grid forming converter contributes with 2/3 of the load and the other 1/3, in normal condition the error power is passed through a 2/3 gain and will only contribute with a small amount of power, this is regulated by the synchronous machine. The arrangement is such that one unit takes care of fast frequency- and the other frequency containment reserves.

The magnitude of the disturbance has been increased to 2.5 p.u to induce more frequency deviation, hereby enabling the clarity of this control application. While it may be a cheap approach, it effectively achieves the desired outcome.

It was considered to use a phase locked loop block to detect the angular position at reference frame, but when employing grid-forming converters, a phase locked loop free grid is desirable. Moreover, the power signal is injected into the grid-forming converter. Hereby, the angular position can be taken from the first grid-forming converter. Another solution is to take advantage of the droop, which is a suitable option because the present of powers in the control application. The droop control strategy was applied with the same droop gain coefficient as in droop control in Figure 13. The whole control application is shown Figure 29 - w/droop in the controller Figure 29

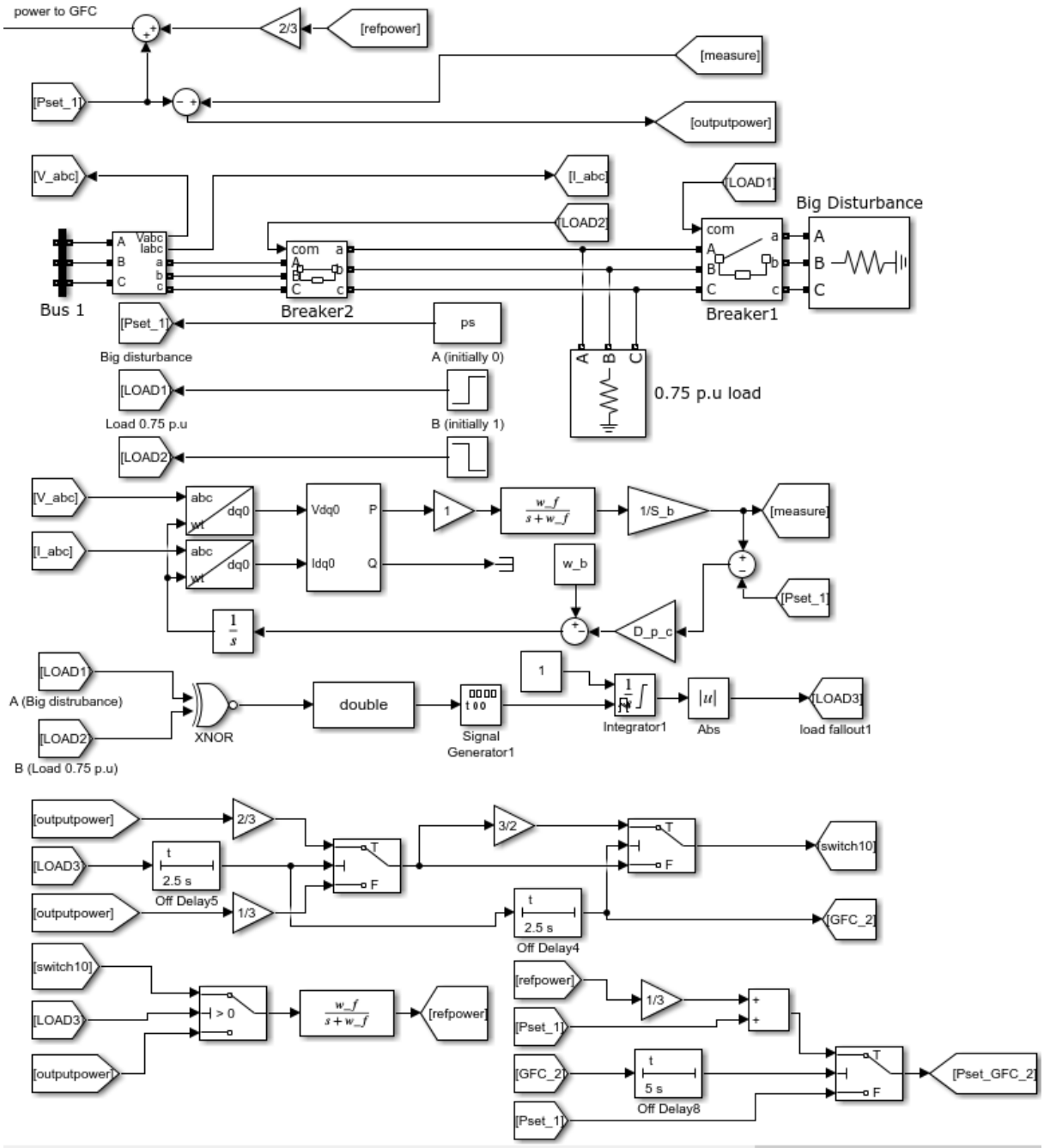

Figure 29 - w/droop in the controller

For simplicity the PS constant and the step responses is placed in the control application, PS is the input of power per unit and is the same as the load in the system. Hereby, as described in the introduction of the model the loads are constant.

4.3 RT-lab model

For the model to be compatible with RT-lab software it needs to be split into at least two subsystems consisting of a master and console. Only the POWRGUI and subsystems of master, slave and console needs to be kept at the top page in order for the RT-lab software to be able to build the model in to its environment. To simplify the process of building models in RT-LAB environments, the base workbench parameters, which are generated by scripts, have been incorporated into the model workbench and remain with the model. This approach eliminates errors and delays that may arise during data transfer, ensuring accuracy.

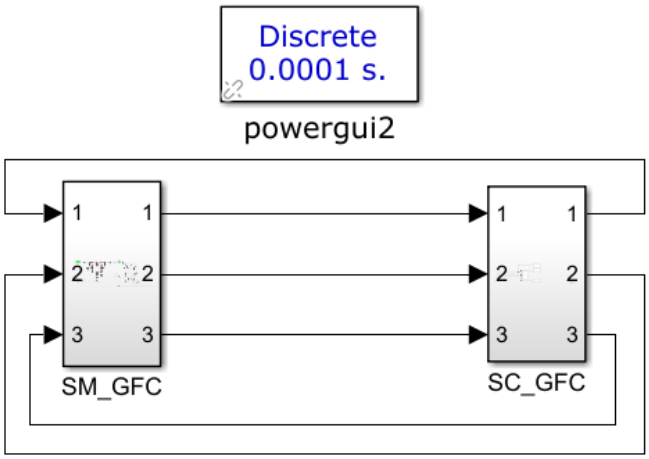

Figure 30 - Top page RT-lab

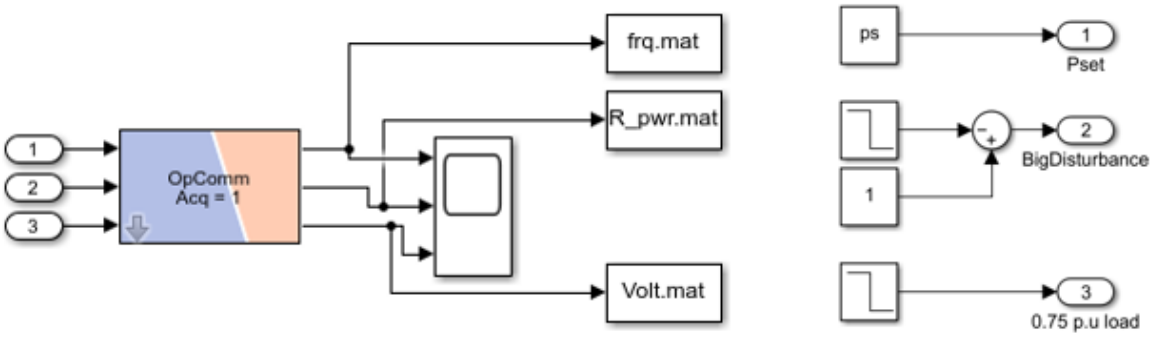

Figure 31 - Console subsystem RT-Lab

The step responses are used to enable the comparison of the same models. For the step response of the large disturbance output, the signal should initially be set to 0, but then it becomes single, the datatype should be double since the other signals transferred through the OpComm block is a double datatype. Hereby, the reversed step response. Moreover, the step

blocks can be changed to constants, allowing the user to interact with the system live if desired. The master subsystem consists of the model itself and the control application shown in Figure 32

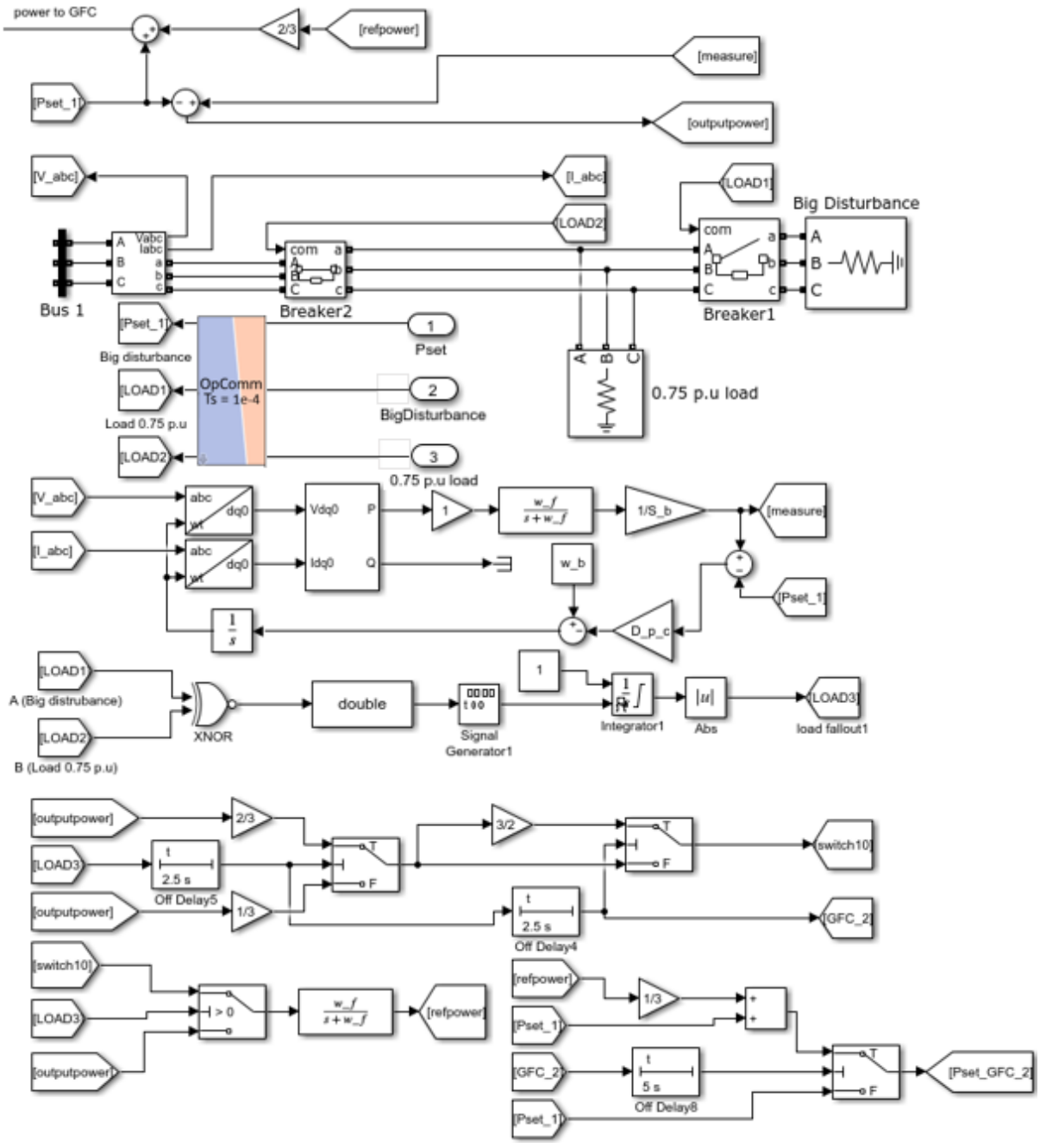

Figure 32 - Control application in the Master Subsystem RT-lab

Due to the complexity of the models, increasing the POWERGUI time Ts to slow down the system was not possible, as there were too many interactions happening simultaneously, which will cause the system to crash. However, in the RT-LAB environment, the system responses did not manage to track Simulink simulations correctly, in contrast deviations appearing to be correct, whereas response was four times faster than with Simulink. There were also given a try to put the nine-bus system without generator sources in a slave subsystem, to see if the system would behave differently, but running it over multiple cores ran the system faster. Since the RT-LAB system requires fixed-step simulations, both the RT-LAB and Simulink models are configured to run with a fixed-step ODE8 solver.

5 Simulations

The tests of the models will consist of these simulations in Simulink and RT-LAB

- One grid-forming converter handles fast frequency- and the other frequency containment reserves.
  - Frequency response
  - Power ratings
  - Voltages
- The synchronous machine handles fast frequency- and one grid-forming converter frequency containment reserves.
  - Frequency response
  - Power ratings
  - Voltages
- Combination of two different grid-forming converters
  - Frequency response
  - Power ratings
  - Voltages

6 Results

6.1 Grid-forming converters frequency regulations

6.1.1 Frequency RT-LAB

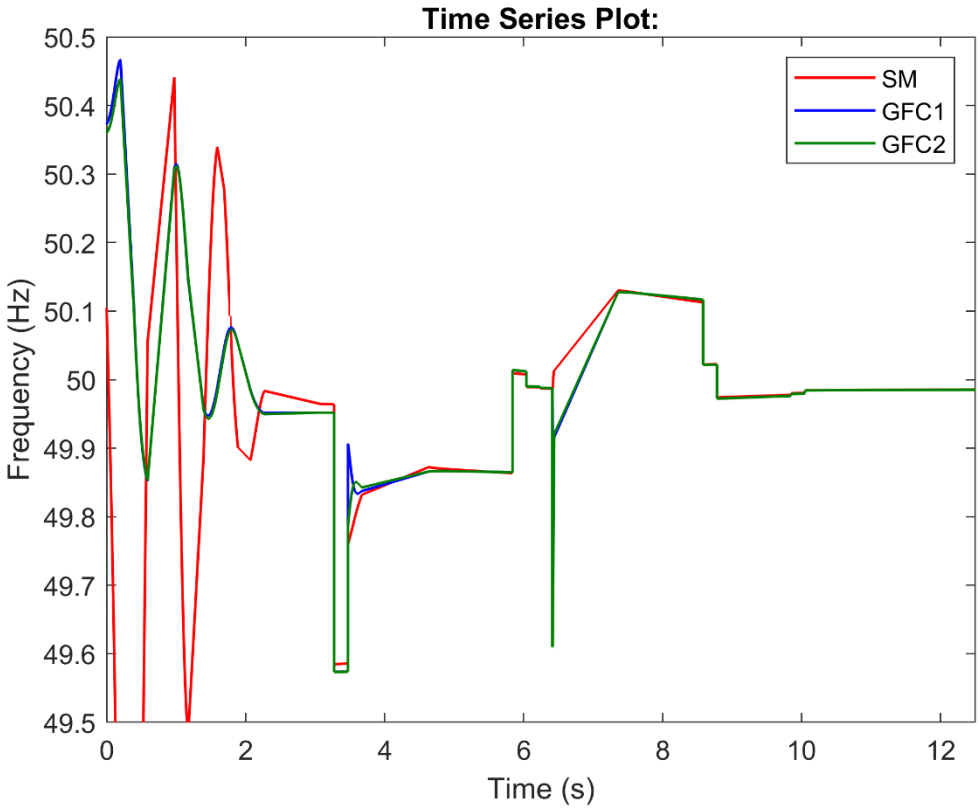

Figure 33 - RT-LAB the frequency response for droop control.

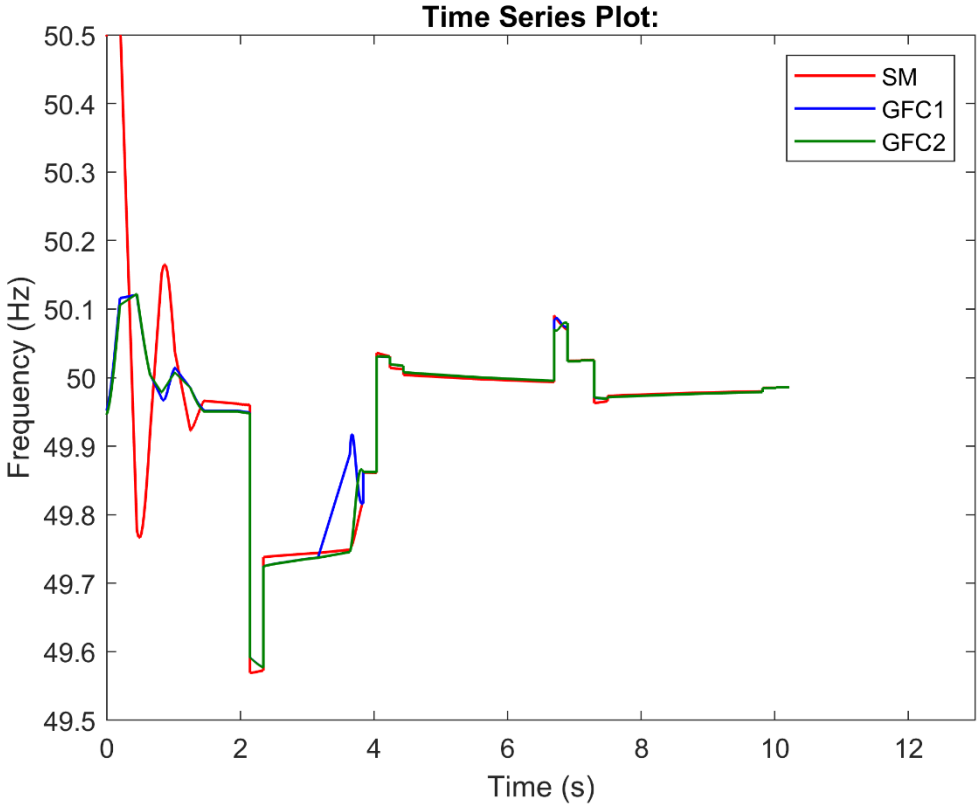

Figure 34 - RT-LAB the frequency response for virtual synchronous machine.

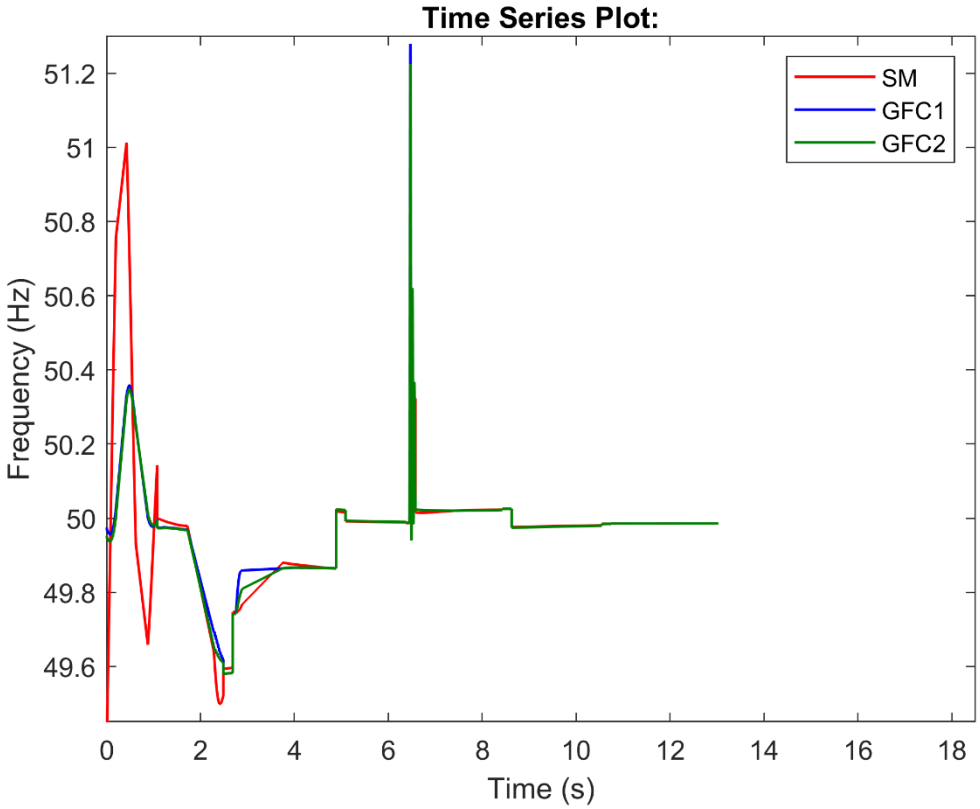

Figure 35 - RT-LAB the frequency response for matching control

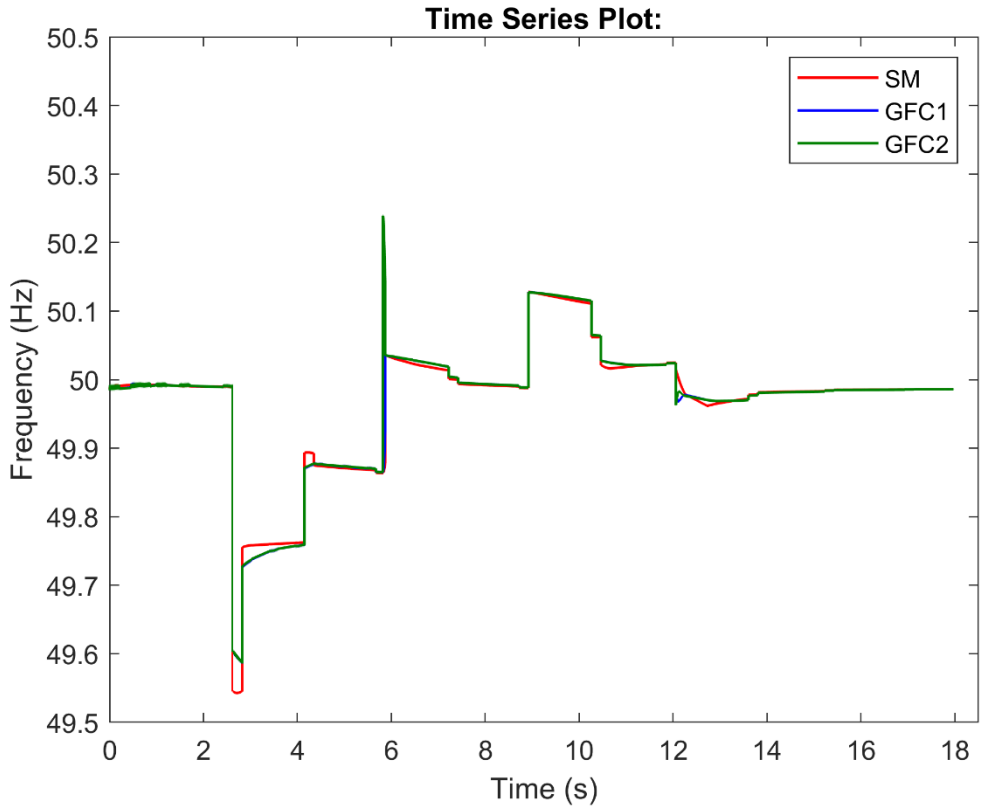

Figure 36 - RT-LAB the frequency response for dispatchable virtual oscillator control.

From Figure 33 to Figure 36, the rate of change of frequency and nadir are quite similar for droop, dispatchable virtual oscillator control, and virtual synchronous machine. However, there are more transient peaks in the Matching model when the load production is increased by 0.75 p.u. The dispatchable virtual oscillator control method managed to track the Simulink simulations more accurately compared to the other grid-forming converter methods. Although the timing is not perfect, the converters seem to be able to follow the same frequency outside the switching periods.

6.1.2 Frequency Simulink

The frequency simulations of all grid-forming converter methods were quite similar, with the only difference being the time it takes for settling when Nadir is reached. In this regard, dispatchable virtual oscillator control stands out as it returns to steady state faster, although all the regulations remain the same (the other plots are shown in the appendix). When there is a loss of power in the system, the frequency amplitude exhibits a higher transient peak compared to when introducing more load to the system.

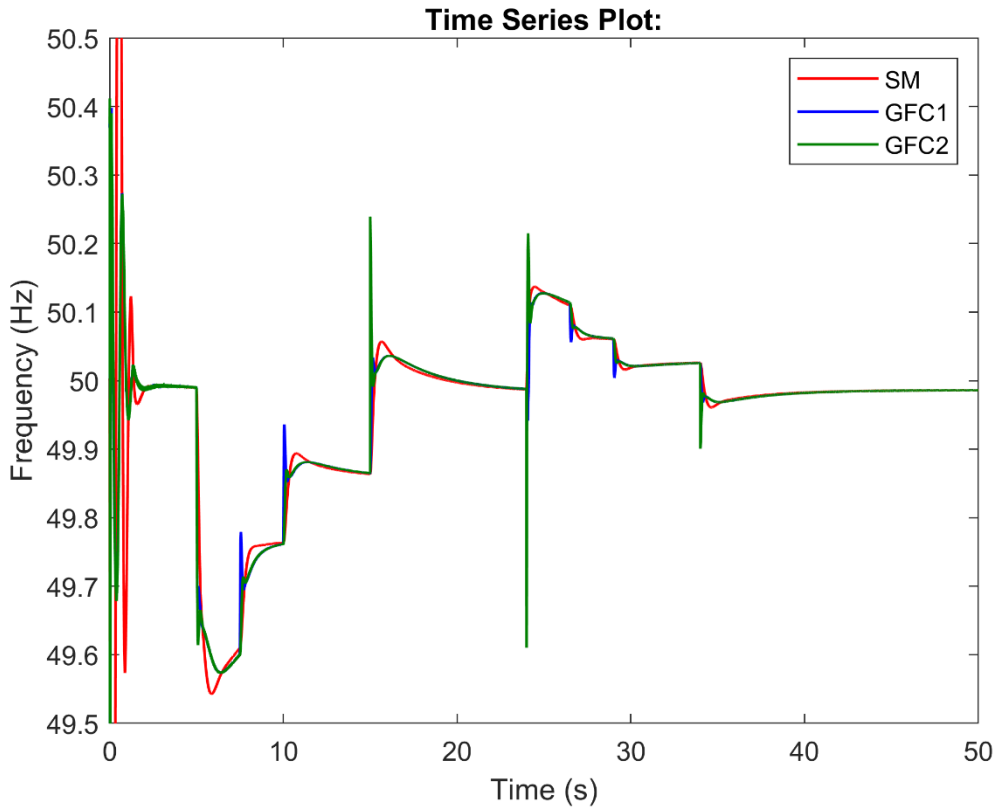

Figure 37 - Simulink the frequency response for dispatchable virtual oscillator control.

6.1.3 Power injections RT-lab

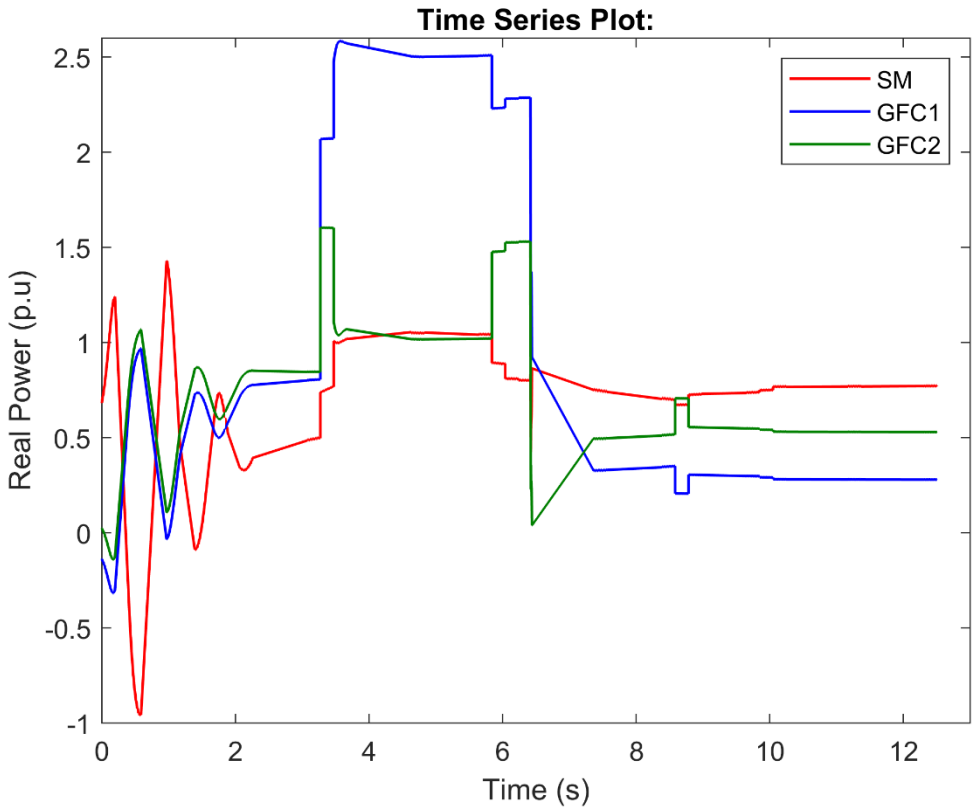

Figure 38 - RT-LAB the real power response for droop control

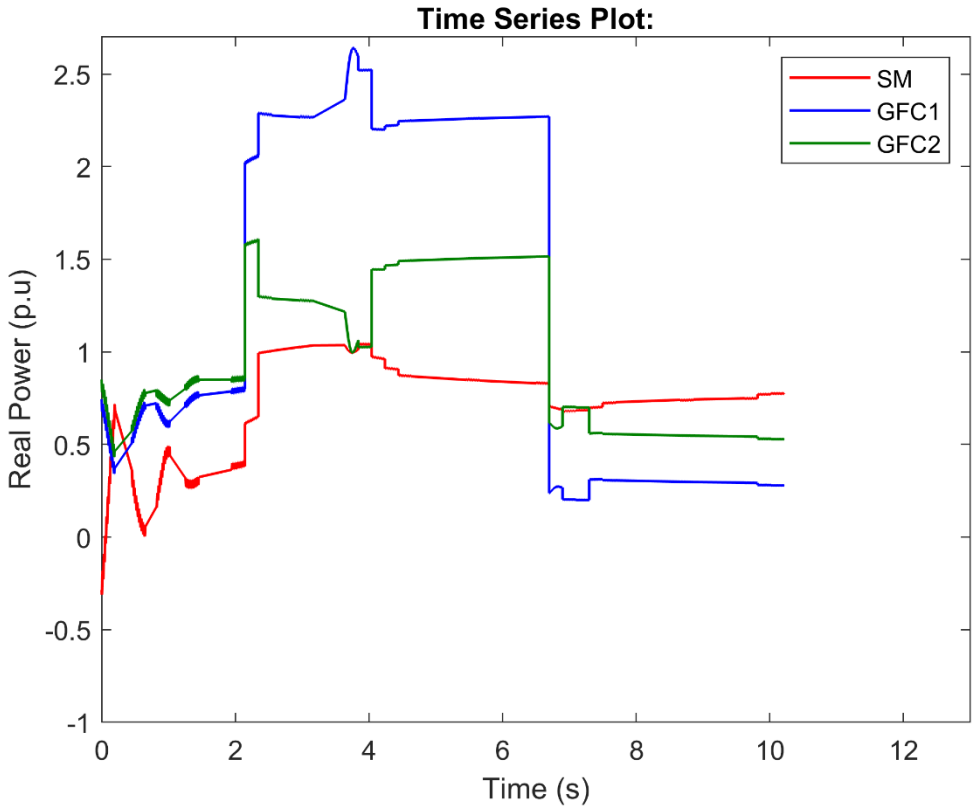

Figure 39 - RT-LAB the real power response for virtual synchronous machine.

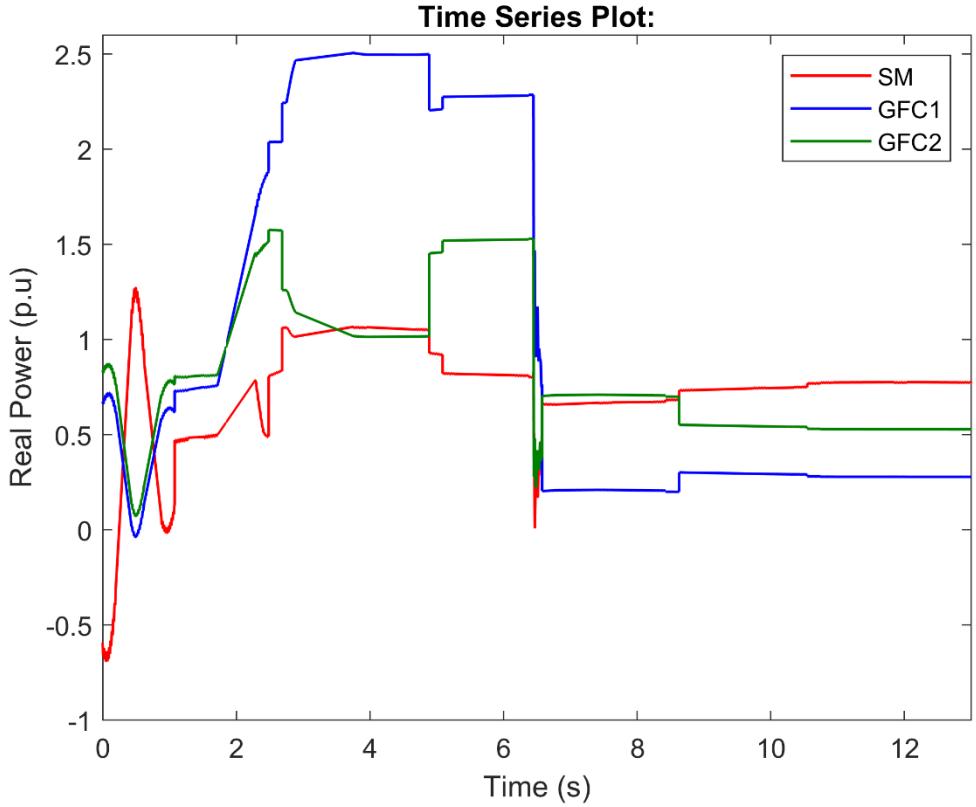

Figure 40 - RT-LAB the real power response for matching control

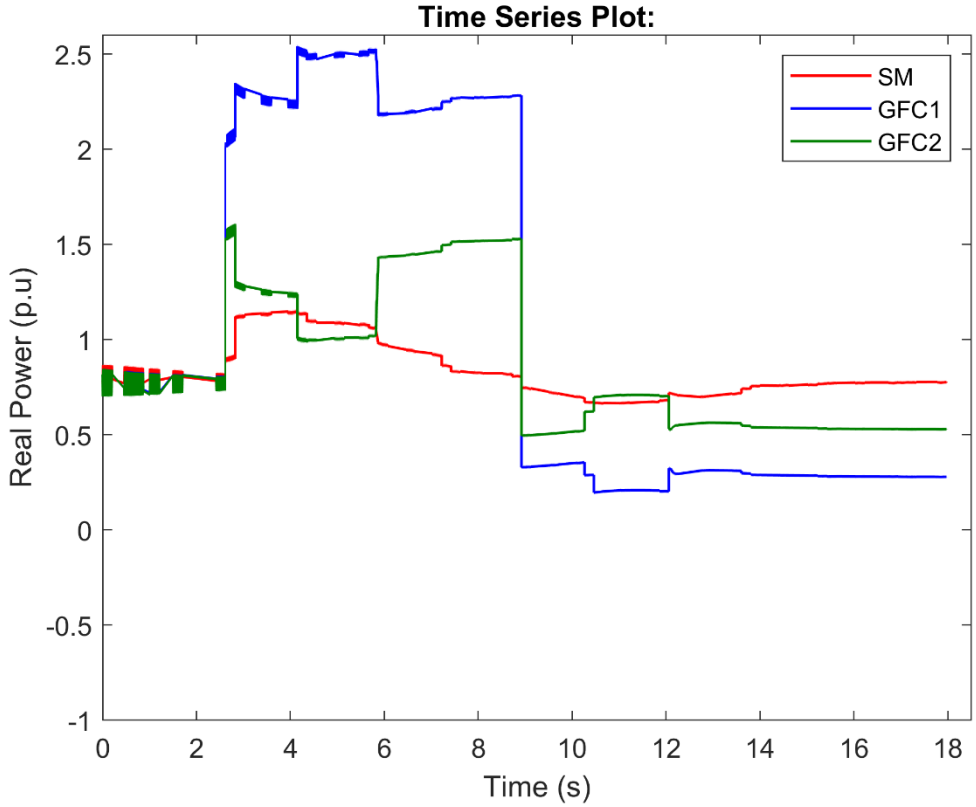

Figure 41 - RT-LAB the real power response for dispatchable virtual oscillator control.

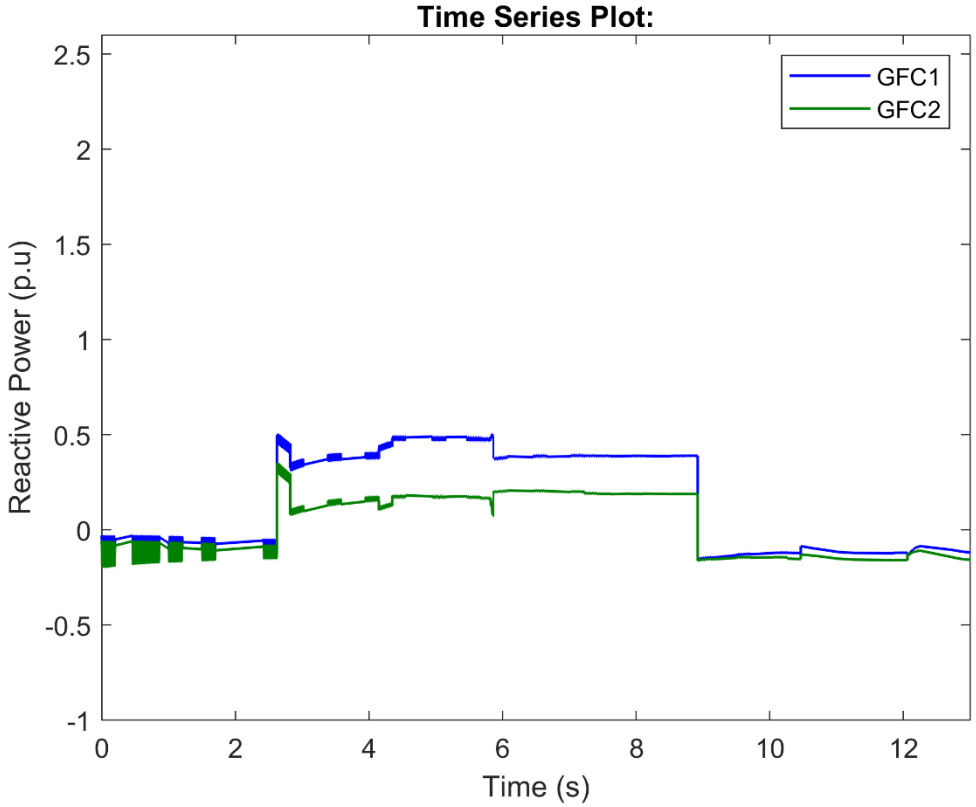

Figure 42 – RT-LAB the reactive power response for dispatchable virtual oscillator regulator

6.1.4 Power injections Simulink

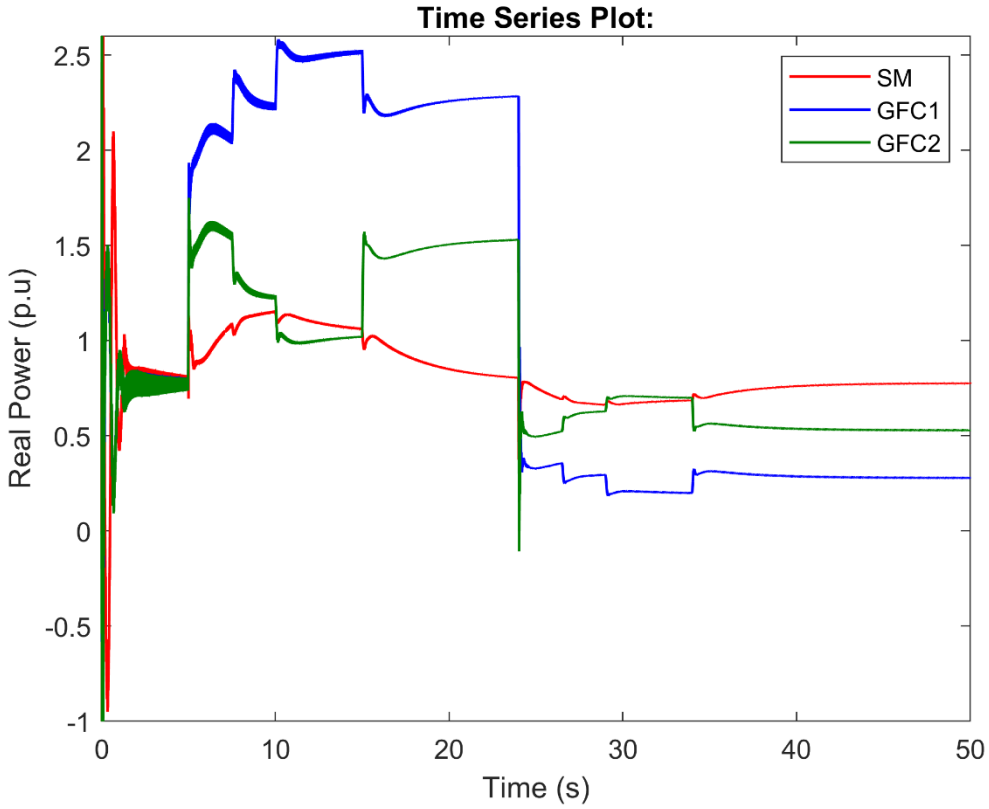

Figure 43 – Simulink the real power response for dispatchable virtual oscillator control.

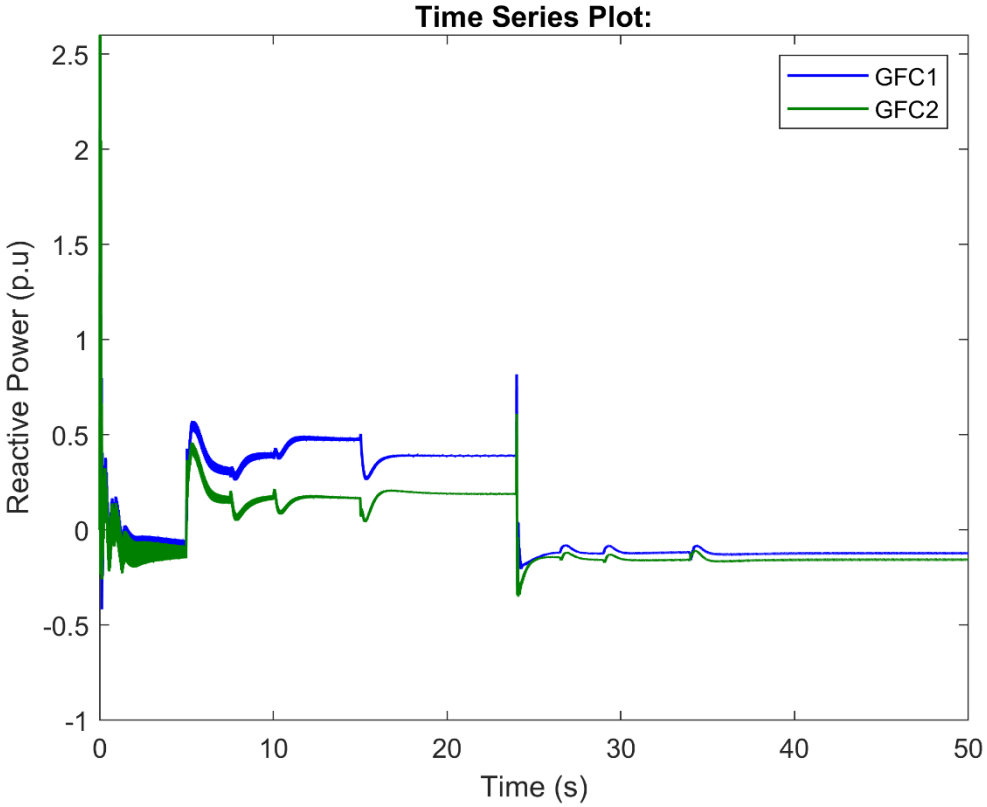

Figure 44 - Simulink the reactive power response for dispatchable virtual oscillator control.

The power response varies significantly in terms of injections among the different grid-forming converter methods. All the different types exhibit rapid dynamics, except for the Matching control, which attempts to mimic the slower inertia response of synchronous generators. The dispatchable virtual oscillator control method shows a lot of oscillations in both real and reactive power outputs. This behavior appears to be when the demand and production are not fully balanced, not until the system settles at steady-state or when production exceeds consumption.

6.1.5 Voltages RT-Lab

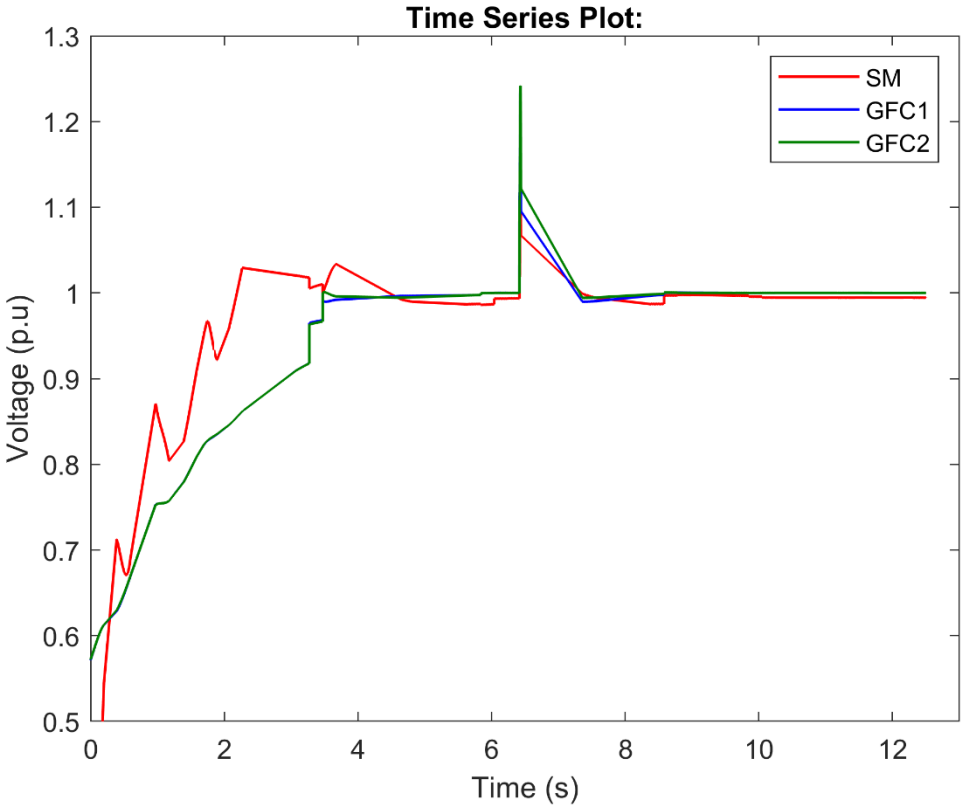

Figure 45 - RT-LAB voltage response droop control.

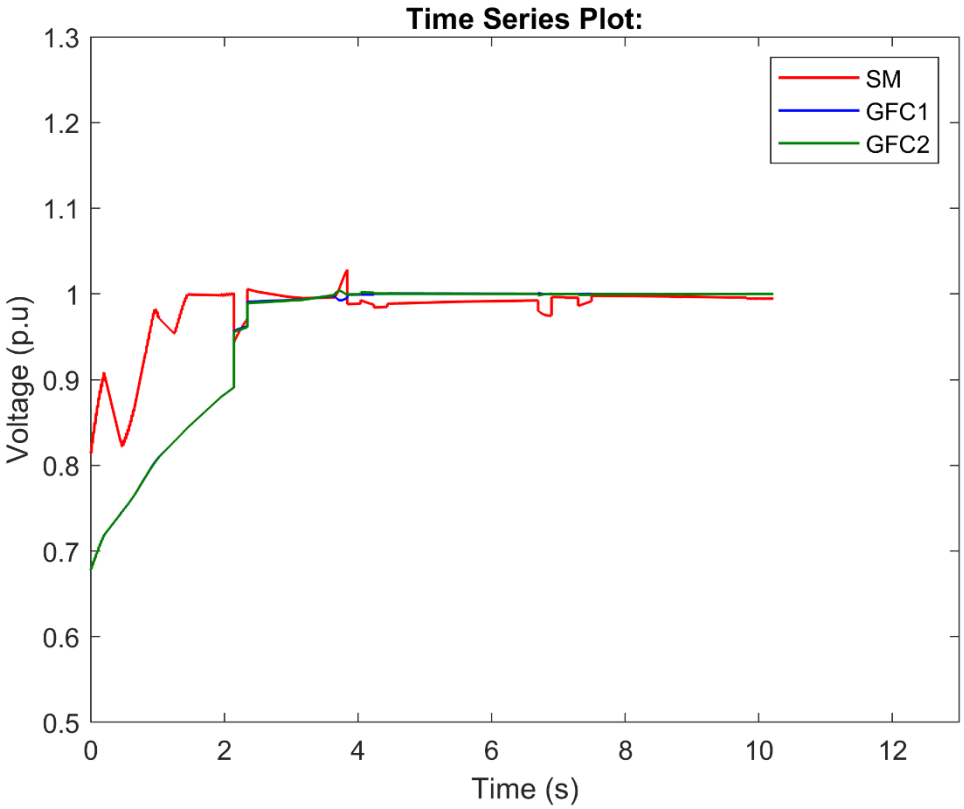

Figure 46 - RT-LAB voltage response virtual synchronous machine.

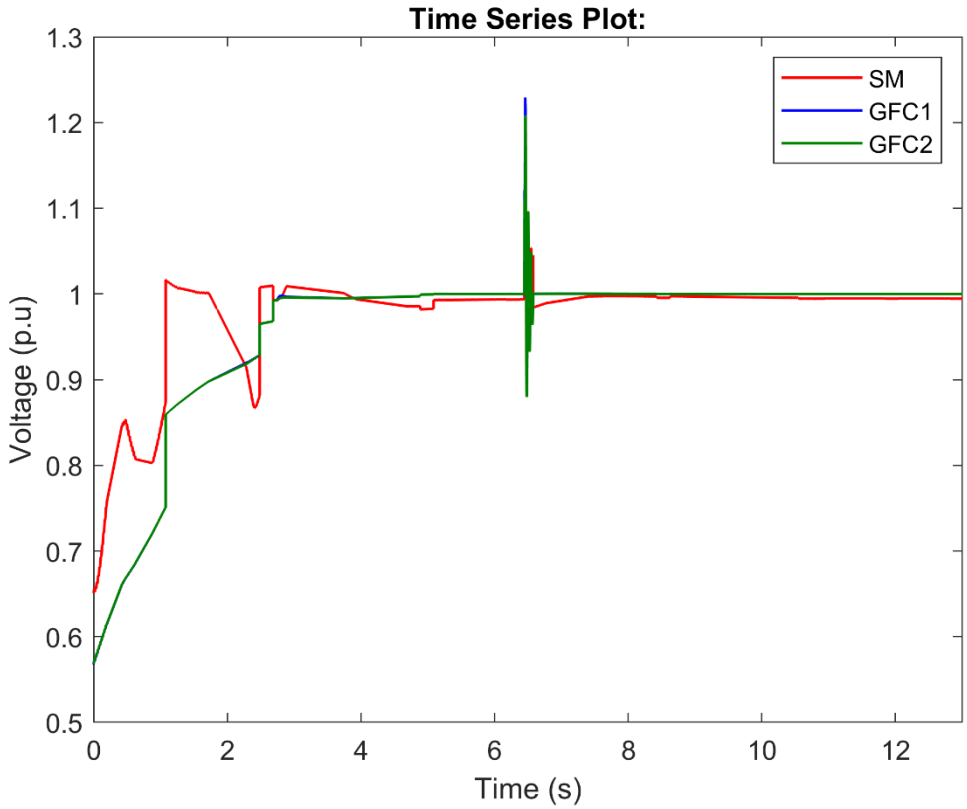

Figure 47 - RT-LAB voltage response matching control.

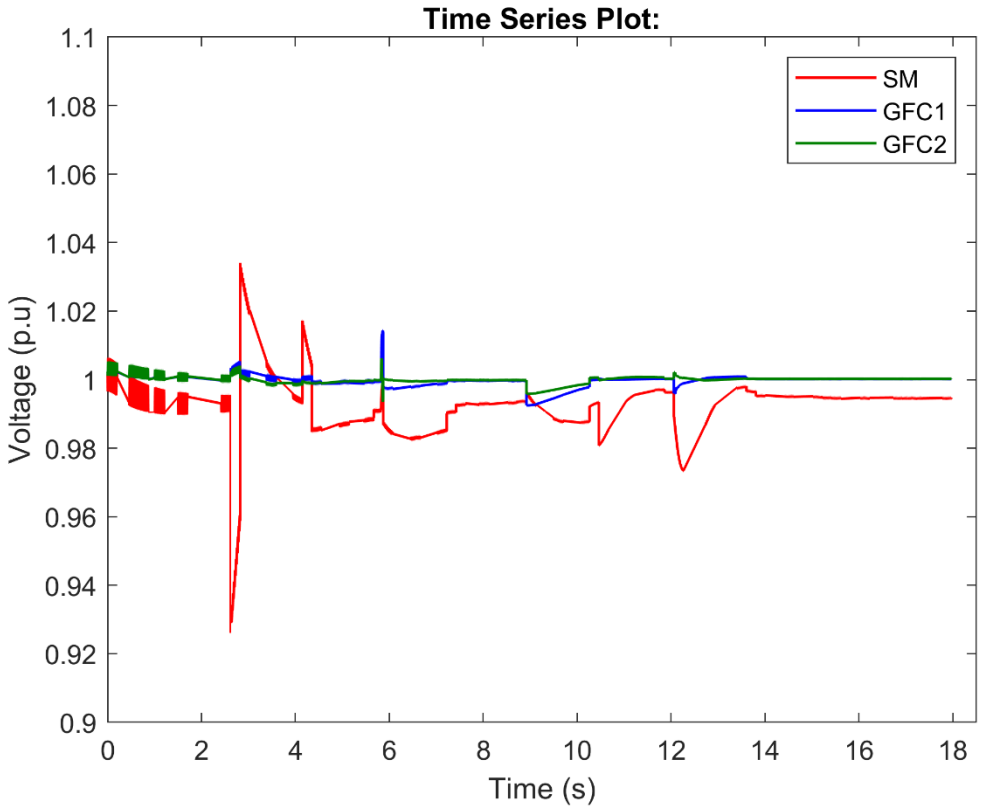

Figure 48 - RT-LAB voltage response dispatchable virtual oscillator control.

In the first three grid-forming converters, the voltage appears to synchronize with the grid when a fault occurs. This synchronization is achieved through the voltage loop control inside the regulating loop. After the fault is resolved, the voltage remains synchronized, except in the case of a load loss. During fault events, the transient peaks in voltage deviation are quite large per unit. Additionally, the dispatchable virtual oscillator control method effectively maintains stable output voltage at its bus despite deviations, although the synchronous machine regulate more. This difference seems like it is related to the reactive power injections from the dispatchable virtual oscillator control.

6.1.6 Voltages Simulink

There are more oscillations in the voltage before the fault occurs in the RT-LAB simulations compared to Simulink. In contrast, the deviation in the Simulink model is larger.

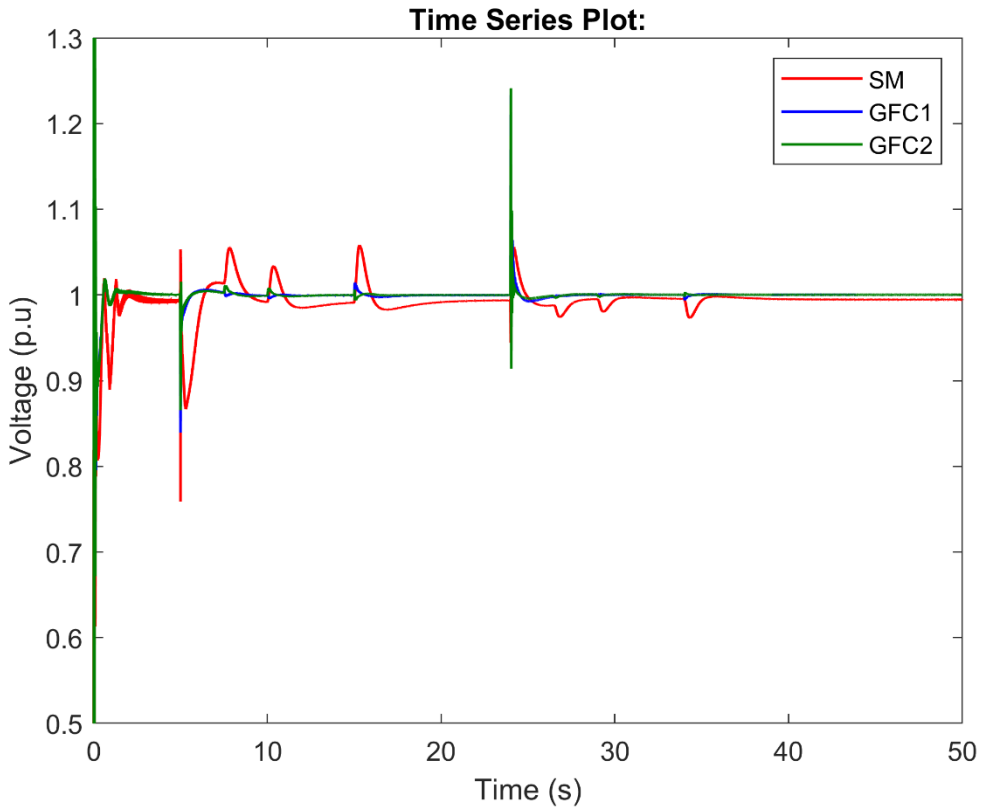

Figure 49 – Simulink voltage response dispatchable virtual oscillator control

6.2 Synchronous machine as main regulator

The synchronous machine is employed for fast frequency response, while the virtual synchronous machine for frequency containment reserves. This can be seen from Figure 53.

6.2.1 RT-LAB simulation

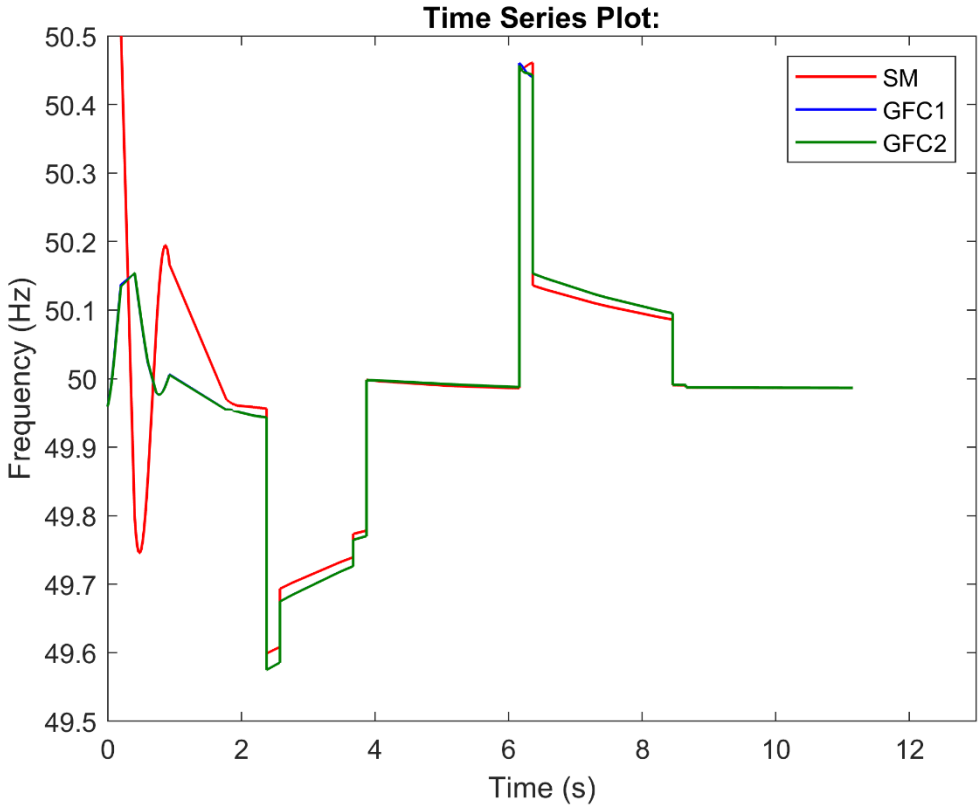

Figure 50 - RT-LAB frequency response Synchronous machine main regulator

An expected slope can be observed in the synchronous generator dynamics, indicating its inertia properties, this can be seen in the Figure 50. In contrast, the virtual synchronous machine converter exhibits a rapid response. Moreover, there are no transient peaks during switching, which is an indication of stability compared to the other results.

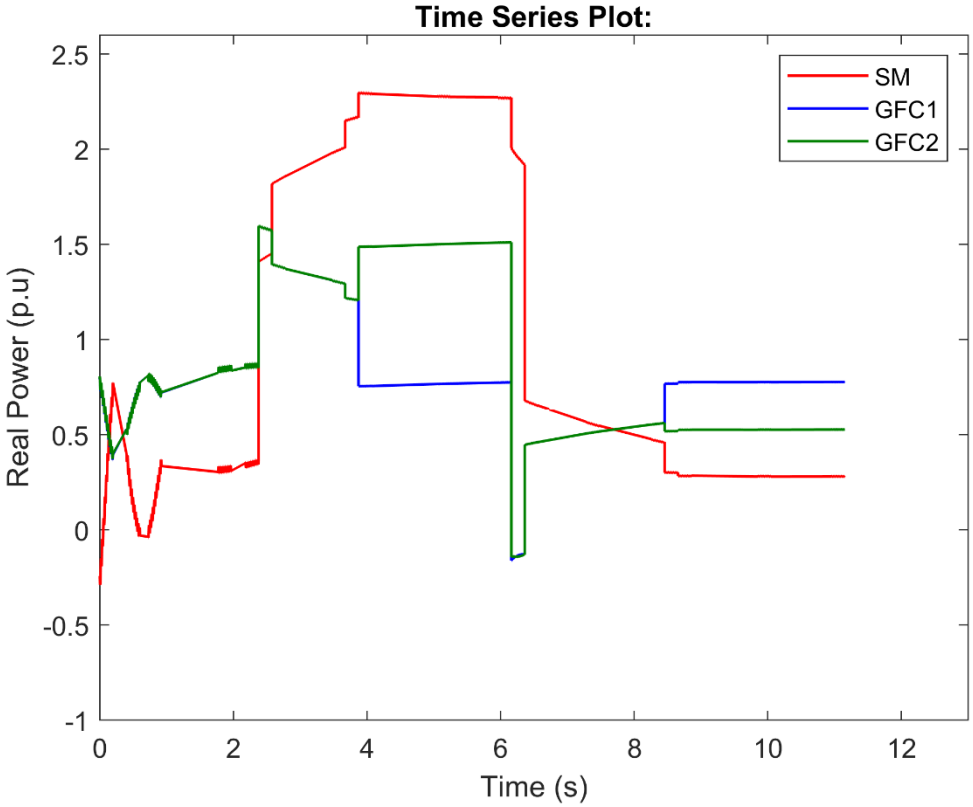

Figure 51 - RT-LAB power response synchronous machine main regulator

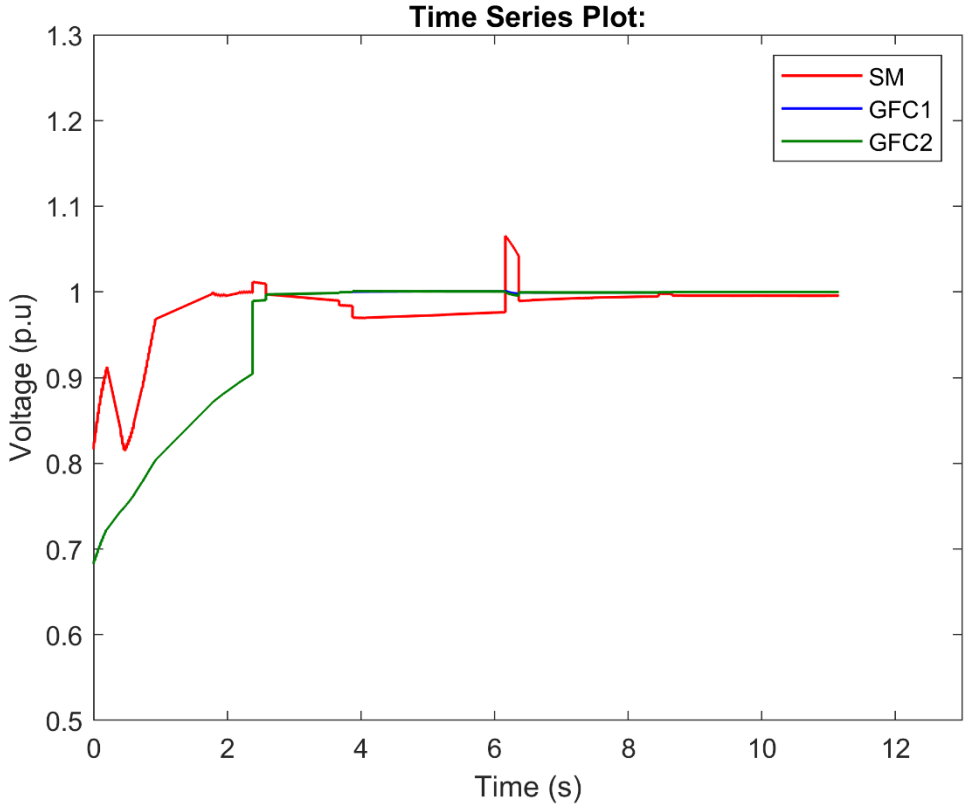

Figure 52 - RT-LAB voltage response Synchronous machine main regulator.

6.2.2 Simulink simulation

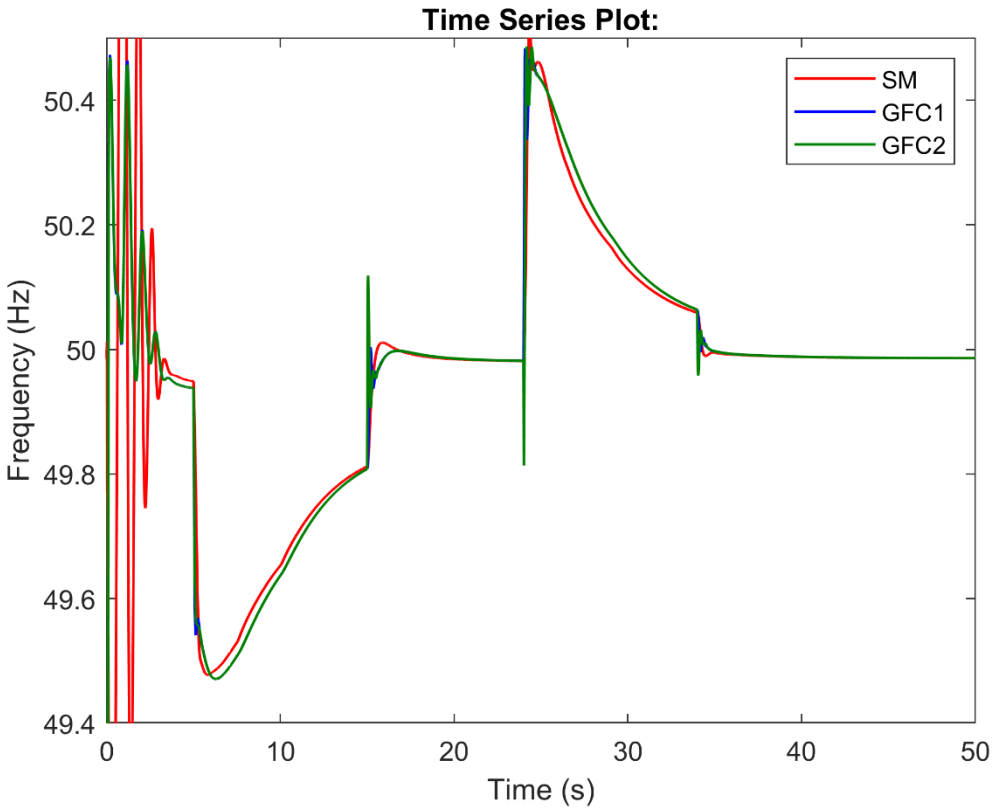

Figure 53 - Simulink frequency response synchronous machine main regulator.

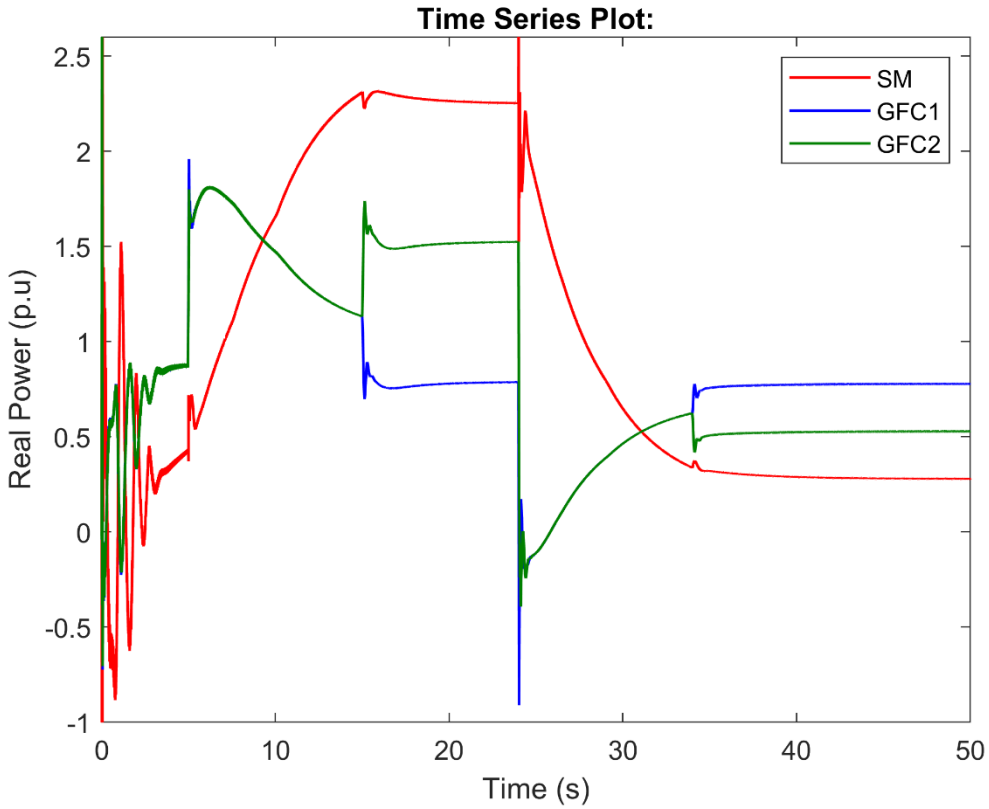

Figure 54 - Simulink power response Synchronous machine main regulator.

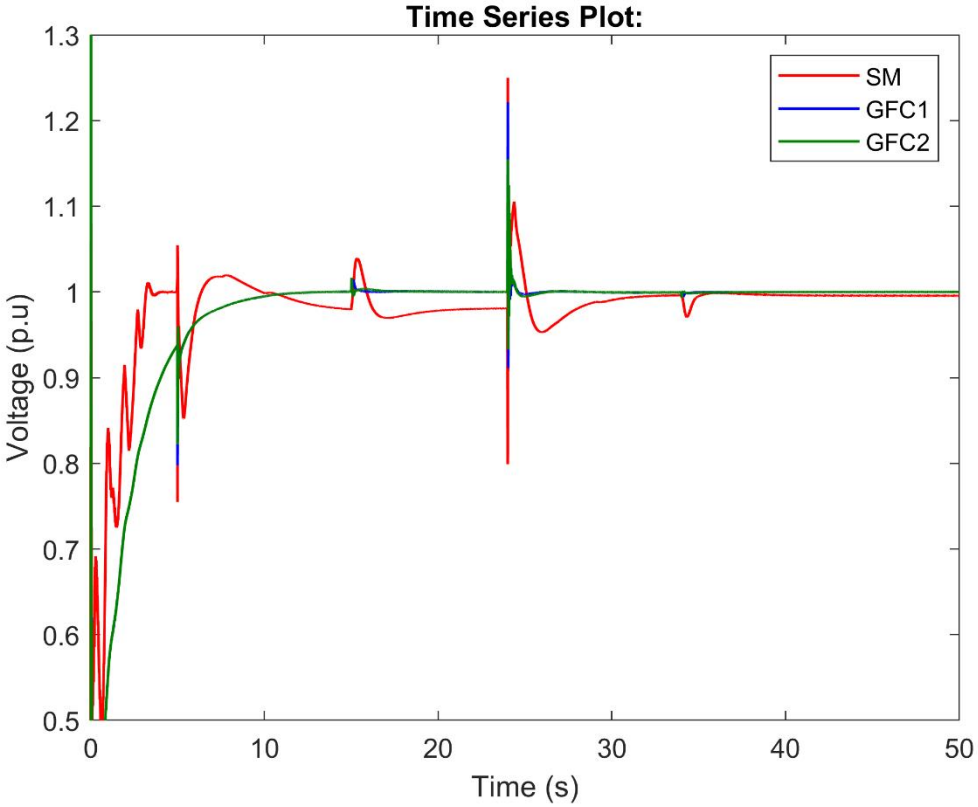

Figure 55 -Simulink voltage response Synchronous machine main regulator.

6.3 Combination of two different Grid-forming converters

The two best combinations of different grid-forming converters results are presented, which consist of the synchronous machine with matching- and droop control applied as generating sources.

6.3.1 RT-LAB simulation

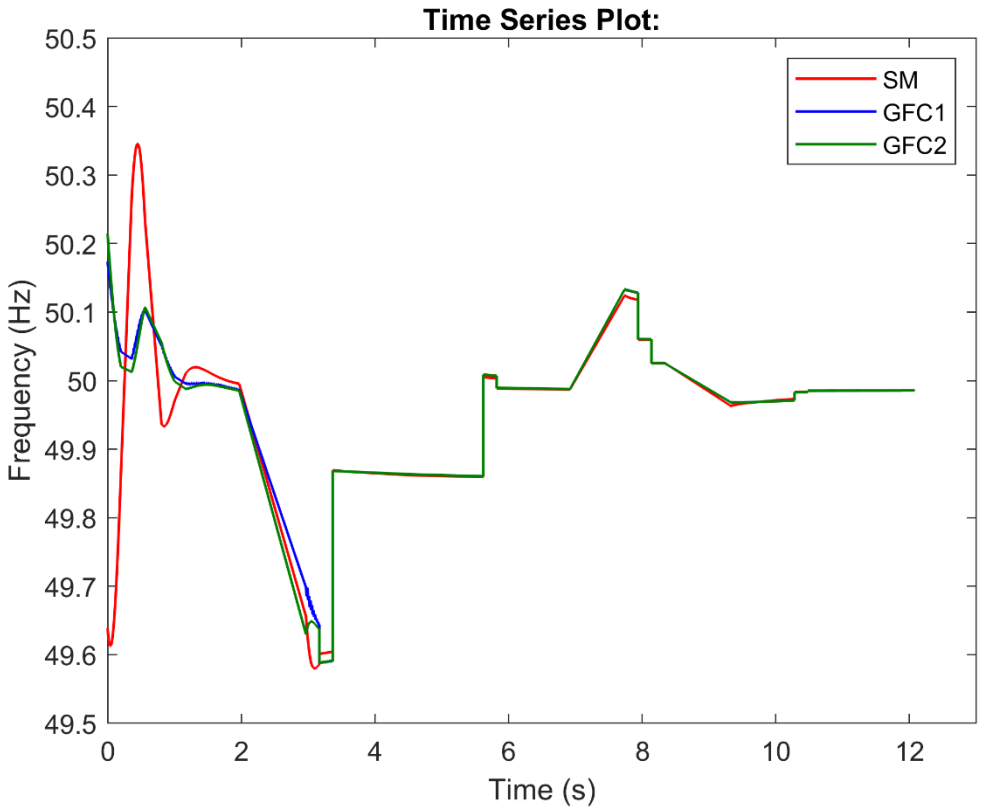

Figure 56 - RT-LAB frequency response of three different generating sources.

In Figure 56, the frequencies for the three different generating sources track each other quite well after nadir, and the power injections closely resemble the behavior of the synchronous machine (Figure 57). The voltage after the post-fault period appears to remain balanced throughout the other events, indicating that the voltage loop has effectively maintained it at a steady state. In contrast, the Simulink model exhibits a transient peak when the fault occurs.

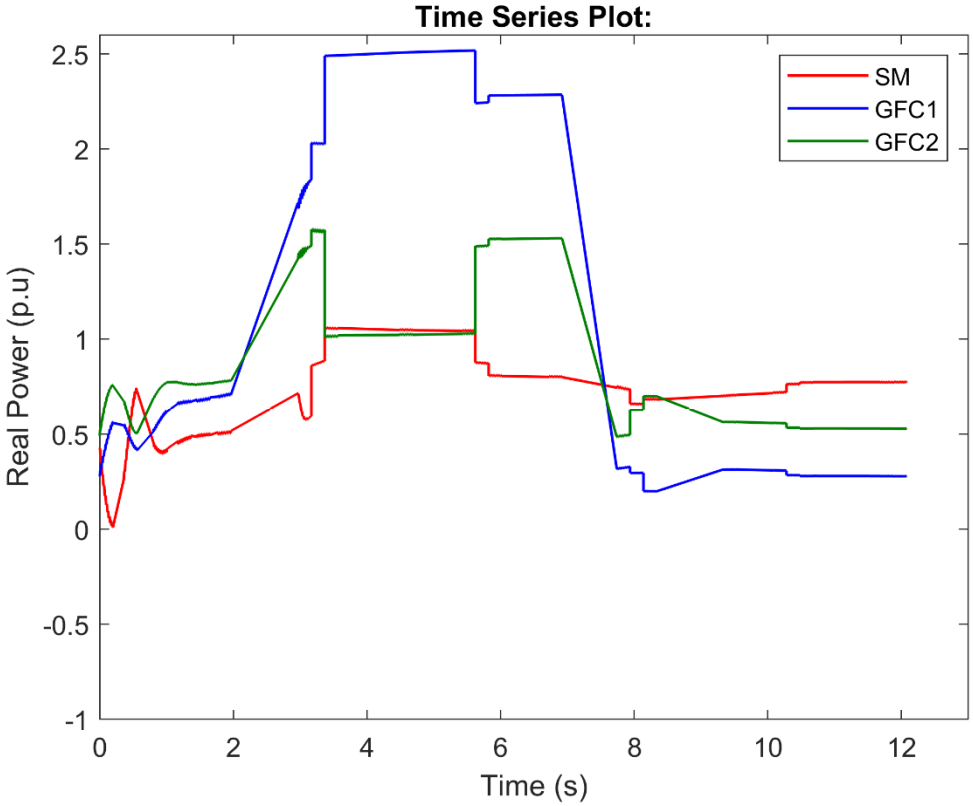

Figure 57 - RT-LAB power response of three different generating sources.

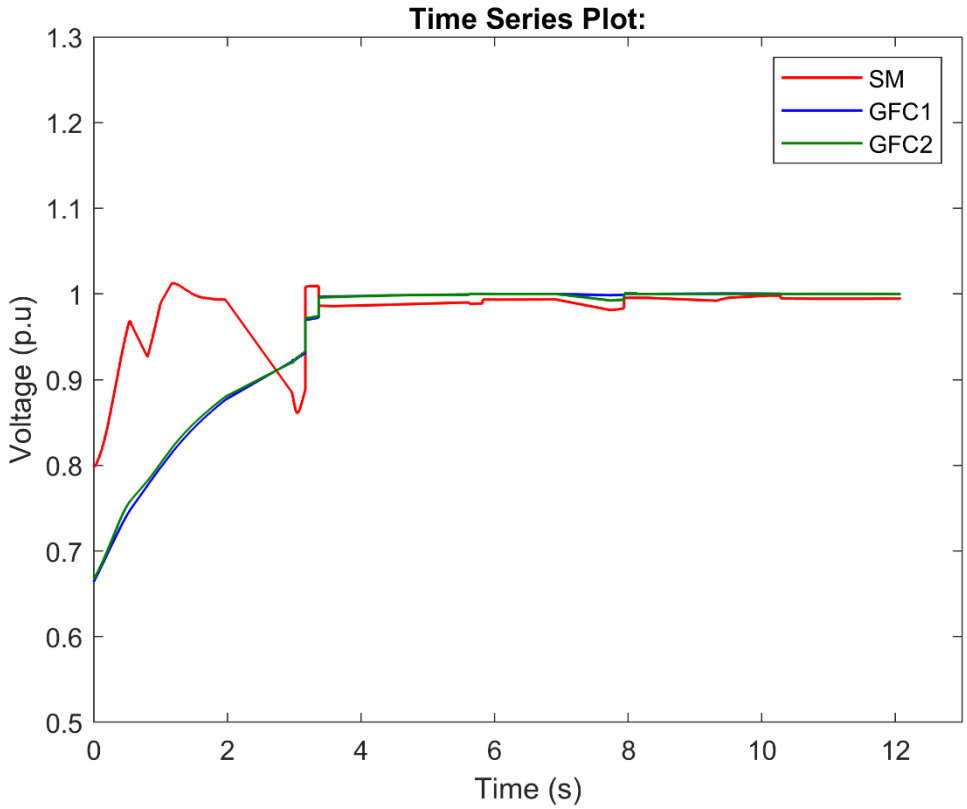

Figure 58 - RT-LAB voltage response of three different generating sources.

6.3.2 Simulink simulation

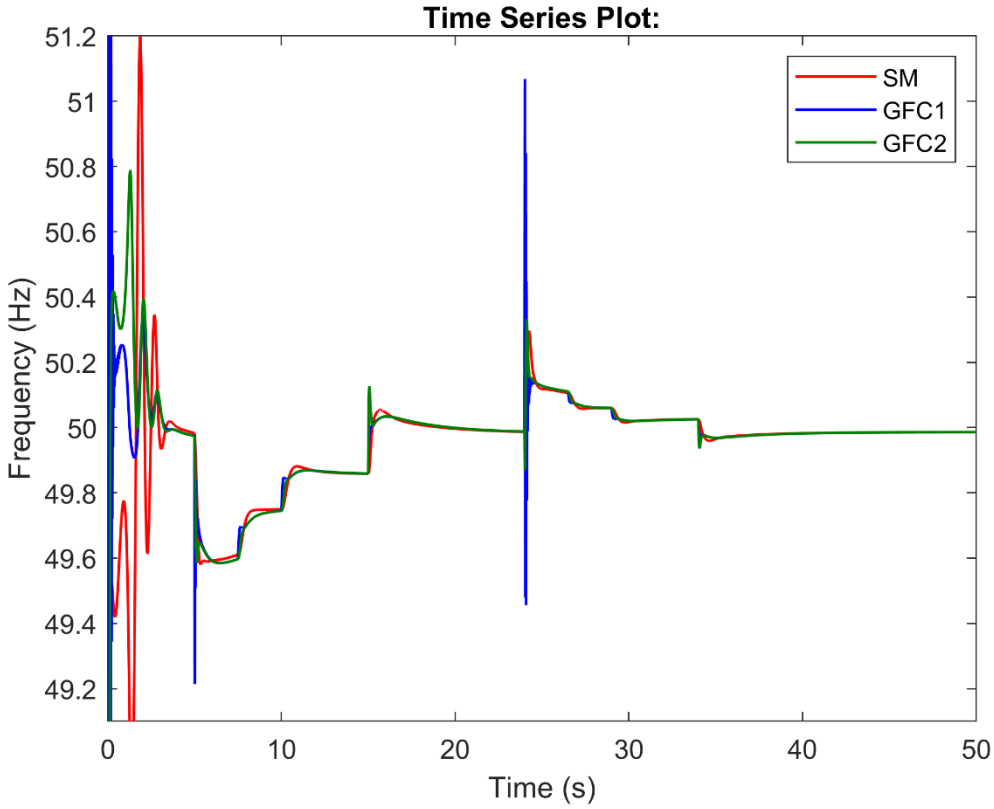

Figure 59 - Simulink frequency response of three different generating sources

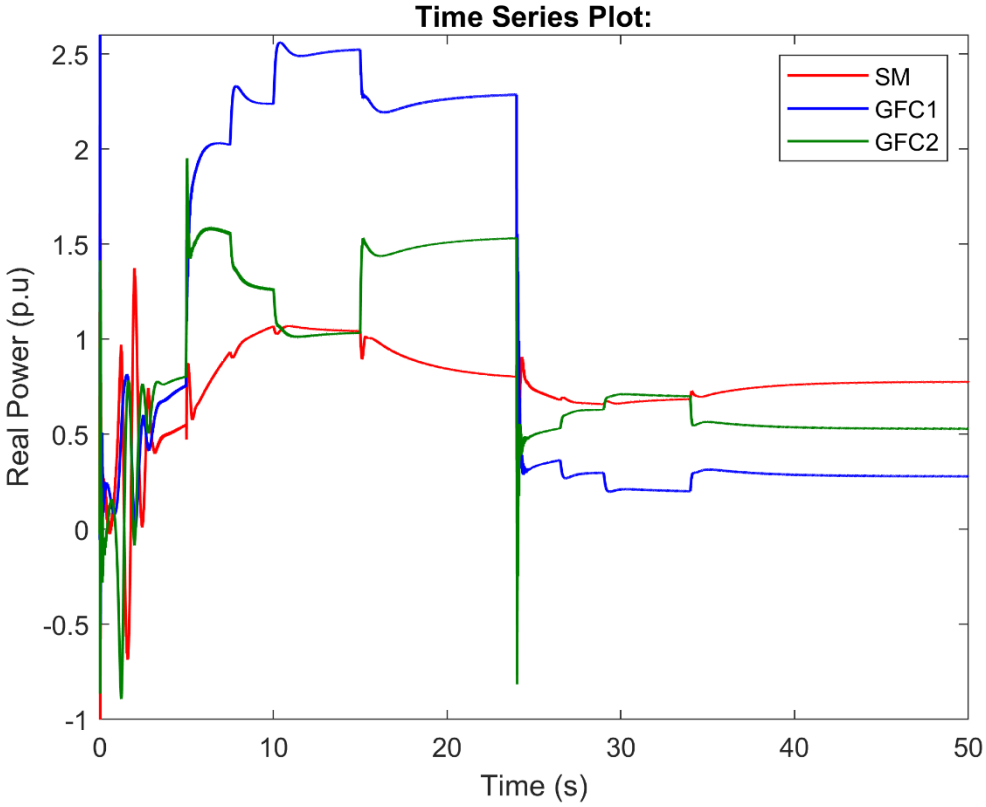

Figure 60 - Simulink power response of three different generating sources

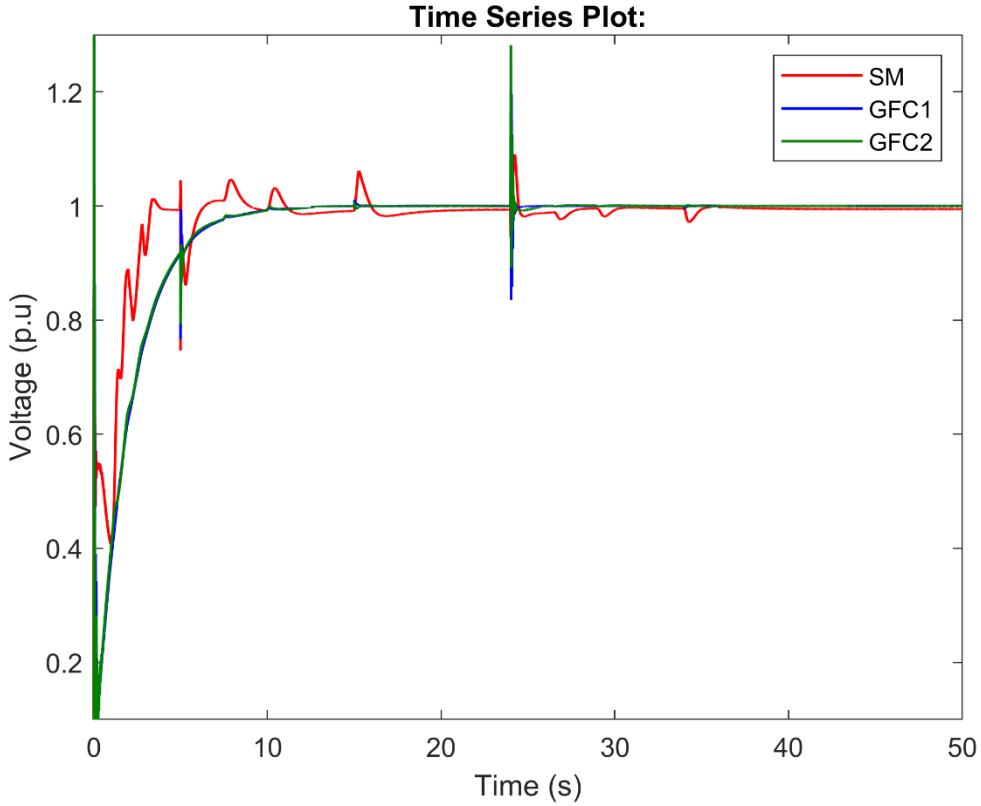

Figure 61 - Simulink voltage response of three different generating sources

7 Conclusion

7.1 Discussion

In this thesis, a study on the dynamic behaviors of four different grid-forming converters under various conditions in a nine-bus system is analyzed. It is shown that grid-forming converters can operate as frequency regulators, depending on the available power source and careful tuning. To address this, a possible solution is to avoid running the generator sources at maximum power and keep some in standby in case of sudden big changes, thus overcoming outages in their area. The rapid dynamics of these converters have demonstrated that they do not have the slow startup time characteristic of synchronous generators before reaching their desired power output. Some applications exhibited rapid response, while others were slower, with high transient peaks observed during disturbances in both Simulink and RT-LAB simulations. The voltage loop control effectively managed the resolve the error during the faults and synchronized the grid-forming converters to the grid voltage in the real-time simulator. Timing events outside the loops were found to be up to 10 times faster in RT-LAB compared to Simulink.

7.2 Future Work

For future work the models could be optimized in both RT-LAB and Simulink by simplifying complex subsystems, remove unnecessary components to improve simulation performance and computational error. Furthermore, investigate the integration of energy storage systems with grid-forming converters to enhance their capability for grid support and stability. This could involve studying battery energy storage systems with control strategies for coordination between grid-forming converters and these storage systems. Additionally, introducing the grid-forming converters to high voltage direct current transmission lines systems or augment the system with more inductive loads.

Bibliography

[1] ATayebi, “GitHub - ATayebi/GridFormingConverters: Implementation of Grid-Forming Control Techniques in IEEE 9-Bus System.” May 2020. [Online]. Available: https://github.com/ATayebi/GridFormingConverters

[2] A. T, “Power System Stability,” *Circuit Globe*, May 2017, [Online]. Available: https://circuitglobe.com/power-system-stability.html

[3] J. Machowski, J. W Bialek, and J. R Bumby, *Power System Dynamics: stability and control*, 2nd ed. Southern Gate, Chichester, gb: John Wiley & Sons Ltd, 2008.

[4] “Factsheet Transmission system operators,” May 2015, [Online]. Available: https://renewables-grid.eu/fileadmin/user_upload/Files_RGI/RGI_Publications/Factsheets/RGI_Factsheet_TSO.pdf .

[5] P. Kundur, *Power System Stability and Control*. New York, us: McGraw-Hill Companies, 1994.

[6] “Frequency Stability and Control in Smart Grids.” 2019. [Online]. Available: https://smartgrid.ieee.org/bulletins/september-2019/frequency-stability-and-control-in-smart-grids

[7] Z. Zhou, W. Wang, T. Lan, and G. M. Huang, “Dynamic Performance Evaluation of Grid-Following and Grid-Forming Inverters for Frequency Support in Low Inertia Transmission Grids,” May 2021. doi: 10.1109/isgteurope52324.2021.9640034.

[8] H. W. Shin, J. Jung, and B. Lee, “Determining the Capacity Limit of Inverter-Based Distributed Generators in High-Generation Areas Considering Transient and Frequency Stability,” *IEEE Access*, vol. 8, pp. 34071–34079, May 2020, doi: 10.1109/access.2020.2974481.

[9] E. F. Alves, D. D. S. Mota, and E. Tedeschi, “Sizing of Hybrid Energy Storage Systems for Inertial and Primary Frequency Control,” *Front Energy Res*, vol. 9, May 2021, doi: 10.3389/fenrg.2021.649200.

[10] “Fast Frequency Reserve – Solution to the Nordic inertia challenge,” May 2019. [Online]. Available: https://www.statnett.no/globalassets/for-aktorer-i-kraftsystemet/utvikling-av-kraftsystemet/nordisk-frekvensstabilitet/ffr-stakeholder-report_13122019.pdf

[11] “Reserves and balancing power.” May 2017. [Online]. Available: https://www.fingrid.fi/en/electricity-market/reserves_and_balancing/#reserve-obligations-and-procurement-sources

[12] O. Andersson, “Inclusion of Wind Turbines into Frequency Support Services Exploring frequency stability issues and comparing regulation power market products .” Uppsala University , 2021. [Online]. Available: http://www.diva-portal.org/smash/get/diva2:1529906/FULLTEXT01.pdf

[13] “Frequency containment reserves (FCR products).” May 2017. [Online]. Available: https://www.fingrid.fi/en/electricity-market/reserves_and_balancing/frequency-containment-reserves/

[14] “Fast Frequency Reserve (FFR).” May 2020. [Online]. Available: https://www.fingrid.fi/en/electricity-market/reserves_and_balancing/fast-frequency-reserve/#technical-requirements

[15] “Automatic frequency restoration reserve (aFRR).” May 2018. [Online]. Available: https://www.fingrid.fi/en/electricity-market/reserves_and_balancing/automatic-frequency-restoration-reserve/

[16] “Balancing energy and balancing capacity markets (mFRR).” May 2018. [Online]. Available: https://www.fingrid.fi/en/electricity-market/reserves_and_balancing/balancing-energy-and-balancing-capacity-markets/

[17] S. Abe, Y. Fukunaga, A. Isono, and B. Kondo, “Power System Voltage Stability,” *IEEE Transactions on Power Apparatus and Systems*, vol. PAS-101, no. 10, pp. 3830–3840, May 1982, doi: 10.1109/tpas.1982.317069.

[18] Y. Levron, J. Belikov, and D. Baimel, “A Tutorial on Dynamics and Control of Power Systems with Distributed and Renewable Energy Sources Based on the DQ0 Transformation,” *Applied sciences*, vol. 8, no. 9, p. 1661, May 2018, doi: 10.3390/app8091661.

[19] “Implement αβ0 to dq0 transform - Simulink - MathWorks Nordic.” [Online]. Available: https://se.mathworks.com/help/sps/ref/clarketoparkangletransform.html

[20] B. Gündoğdu, D. T. Gladwin, S. Nejad, and D. H. Stone, “Scheduling of grid-tied battery energy storage system participating in frequency response services and energy arbitrage,” *Iet Generation Transmission & Distribution*, vol. 13, no. 14, pp. 2930–2941, May 2019, doi: 10.1049/iet-gtd.2018.6690.

[21] “What Is MATLAB?” [Online]. Available: https://se.mathworks.com/discovery/what-is-matlab.html

[22] “RT-Lab Solo: Getting Started User’s Manual ,” May 2003. [Online]. Available: https://www.cim.mcgill.ca/~ialab/members/usefuldoc/RT-Lab_Instructions_v2.11.pdf

[23] A. Dubey, S. Chakrabarti, and V. Terzija, “Testing and validation of a dynamic estimator of states in OPAL-RT real time simulator,” May 2017. doi: 10.1109/pesgm.2017.8273954.

[24] “Subsystems - OPAL-RT.” May 2022. [Online]. Available: https://www.opal-rt.com/de/opal_tutorial/subsystems/

[25] “User Manuals of Former Products - Hardware Products Documentation - Confluence.” 2023. [Online]. Available: https://opal-rt.atlassian.net/wiki/spaces/PHDGD/pages/144657490/User+Manuals+of+Former+Products

[26] P. Roos, “A Comparison of Grid-Forming and Grid-Following Control of VSCs,” 2020. [Online]. Available: https://www.diva-portal.org/smash/get/diva2:1444307/FULLTEXT01.pdf

[27] A. Tayyebi, F. Dörfler, F. Kupzog, Z. Miletic, and W. Hribernik, “Grid-Forming Converters – Inevitability, Control Strategies and Challenges in Future Grids Application,” *CIRED Workshop*, p. 236, May 2018, doi: 10.34890/412.

[28] B. Wen, D. Boroyevich, R. Burgos, P. Mattavelli, and Z. Shen, “Analysis of D-Q Small-Signal Impedance of Grid-Tied Inverters,” *IEEE Trans Power Electron*, vol. 31, no. 1, pp. 675–687, May 2016, doi: 10.1109/tpel.2015.2398192.

[29] “Powering On with Grid-Forming Inverters.” 2021. [Online]. Available: https://www.energy.gov/eere/solar/articles/powering-grid-forming-inverters

[30] S. B. Khan, M. Wang, W. Su, G. Liu, and S. Chaturvedi, “Grid-Forming Converters for Stability Issues in Future Power Grids,” *Energies (Basel)*, vol. 15, no. 14, p. 4937, May 2022, doi: 10.3390/en15144937.

[31] M. Sinha, F. Dörfler, B. F. G. Johnson, and S. V Dhople, “Virtual Oscillator Control subsumes droop control,” May 2015. doi: 10.1109/acc.2015.7171084.

[32] A. Tayyebi, D. GroB, A. Anta, F. Kupzog, and F. Dörfler, “Frequency Stability of Synchronous Machines and Grid-Forming Power Converters,” *IEEE J Emerg Sel Top Power Electron*, vol. 8, no. 2, pp. 1004–1018, May 2020, doi: 10.1109/jestpe.2020.2966524.

[33] P. W. Sauer and M. A. Pai, *Power System Dynamics and Stability*. 1997. [Online]. Available: https://courses.physics.illinois.edu/ece576/sp2018/Sauer%20and%20Pai%20book%20-%20Jan%202007.pdf

[34] I. Ray, “Grid-Forming Converter Control Method to Improve DC-Link Stability in Inverter-Based AC Grids.” 2021. [Online]. Available: https://trace.tennessee.edu/utk_graddiss/6726/

[35] M. C. Chandorkar, D. M. Divan, and R. Adapa, “Control of parallel connected inverters in standalone AC supply systems,” *IEEE Trans Ind Appl*, vol. 29, no. 1, pp. 136–143, May 1993, doi: 10.1109/28.195899.

[36] S. Mansour, M. I. Marei, and A. M. A. Sattar, “Decentralized secondary control for frequency restoration of microgrids with VF and PQ droop controlled inverters,” May 2017. doi: 10.1109/mepcon.2017.8301330.

[37] D. B. Rathnayake *et al.*, “Grid Forming Inverter Modeling, Control, and Applications,” *IEEE Access*, vol. 9, pp. 114781–114807, May 2021, doi: 10.1109/access.2021.3104617.

[38] Q.-C. Zhong and G. H. Weiss, “Synchronverters: Inverters That Mimic Synchronous Generators,” *IEEE Transactions on Industrial Electronics*, vol. 58, no. 4, pp. 1259–1267, May 2011, doi: 10.1109/tie.2010.2048839.

[39] G.-S. Seo, M. Colombino, I. Subotić, B. F. G. Johnson, D. Groß, and F. Dörfler, “Dispatchable Virtual Oscillator Control for Decentralized Inverter-dominated Power Systems: Analysis and Experiments,” May 2019. doi: 10.1109/apec.2019.8722028.

[40] N. Pogaku, M. Prodanović, and T. C. Green, “Modeling, Analysis and Testing of Autonomous Operation of an Inverter-Based Microgrid,” *IEEE Trans Power Electron*, vol. 22, no. 2, pp. 613–625, May 2007, doi: 10.1109/tpel.2006.890003.

[41] Y. Song, D. J. Hill, and T. Liu, “Small-disturbance angle stability analysis of microgrids: A graph theory viewpoint,” May 2015. doi: 10.1109/cca.2015.7320633.

[42] M. C. Shekar and N. Aarthi, “Contingency Analysis of IEEE 9 Bus System,” in *2018 3rd IEEE International Conference on Recent Trends in Electronics, Information & Communication Technology (RTEICT)*, IEEE, May 2018, pp. 2225–2229. doi: 10.1109/RTEICT42901.2018.9012467.

[43] W. J. G. González, “Passivity-Based Control and Stability Analysis for Hydro-Solar Power Systems,” *ResearchGate*, May 2019, [Online]. Available: https://www.researchgate.net/publication/337063591_Passivity-Based_Control_and_Stability_Analysis_for_Hydro-Solar_Power_Systems

[44] “Implement generic power system stabilizer for synchronous machine - Simulink - MathWorks Nordic.” [Online]. Available: https://se.mathworks.com/help/sps/powersys/ref/genericpowersystemstabilizer.html?s_tid=srchtitle_generic%20power_1

Appendix

Simulink and RT-LAB files and plots

There is provided a ZIP-file with the extra data.